

2016

Synthesis of triacetic acid lactone Mannich bases and their inhibition of corrosion

John Rey Apostol Romal
Iowa State University

Follow this and additional works at: <https://lib.dr.iastate.edu/etd>

 Part of the [Chemistry Commons](#)

Recommended Citation

Romal, John Rey Apostol, "Synthesis of triacetic acid lactone Mannich bases and their inhibition of corrosion" (2016). *Graduate Theses and Dissertations*. 15802.
<https://lib.dr.iastate.edu/etd/15802>

This Thesis is brought to you for free and open access by the Iowa State University Capstones, Theses and Dissertations at Iowa State University Digital Repository. It has been accepted for inclusion in Graduate Theses and Dissertations by an authorized administrator of Iowa State University Digital Repository. For more information, please contact digirep@iastate.edu.

Synthesis of triacetic acid lactone Mannich bases and their inhibition of corrosion

by

John Rey Apostol Romal

A thesis submitted to the graduate faculty
in partial fulfillment of the requirements for the degree of
MASTER OF SCIENCE

Major: Organic Chemistry

Program of Study Committee:
George A. Kraus, Major Professor
Brent Shanks
Arthur Winter

Iowa State University

Ames, Iowa

2016

Copyright © John Rey Apostol Romal, 2016. All rights reserved.

DEDICATION

To my family and friends.

TABLE OF CONTENTS

| | |
|--|------|
| DEDICATION | ii |
| LIST OF ABBREVIATIONS | iv |
| ACKNOWLEDGEMENTS | vi |
| ABSTRACT | viii |
| | |
| CHAPTER I. MANNICH REACTIONS OF THE BIO-BASED TRIACETIC ACID LACTONE | 1 |
| 1.1. Introduction | 1 |
| 1.2. Results and Discussion | 19 |
| 1.3. Conclusion | 33 |
| 1.4. Experimental | 33 |
| 1.5. References | 45 |
| | |
| CHAPTER II. CORROSION INHIBITION OF SMALL ORGANIC MOLECULES AND TRIACETIC ACID LACTONE MANNICH BASES | 49 |
| 2.1. Introduction | 49 |
| 2.2. Results and Discussion | 63 |
| 2.3. Conclusion | 73 |
| 2.4. Experimental | 74 |
| 2.5. References | 77 |
| | |
| CHAPTER III. GENERAL CONCLUSIONS | 80 |

LIST OF ABBREVIATIONS

| | |
|-------------------|--------------------------------------|
| ACAT | acyl-CoA cholesterol acyltransferase |
| AcOH | acetic acid |
| CDCl ₃ | deuterated chloroform |
| Cu NP | copper nanoparticle |
| DCE | dichloroethane |
| DHA | dehydroacetic acid |
| DMAD | dimethylacetylenedicarboxylate |
| DMM | dimethoxymethane |
| DMSO | dimethylsulfoxide |
| EA | ethyl acetate |
| E. Coli | <i>Escherichia coli</i> |
| EDG | electron-donating group |
| EG | ethylene glycol |
| EI | electron ionization |
| ESI | electrospray ionization |
| EWG | electron-withdrawing group |
| FDCA | 2,5-furandicarboxylic acid |
| GC | gas chromatography |
| HMF | 5-hydroxymethylfurfural |
| ICP | Inductively Coupled Plasma |
| IE | inhibition efficiency |

| | |
|------|--|
| LRMS | low resolution mass spectrometry |
| MCR | multicomponent reaction |
| MeCN | acetonitrile |
| MHz | megahertz |
| mM | millimolar |
| MS | mass spectrometry |
| NMR | Nuclear Magnetic Resonance |
| OCV | open circuit voltage |
| PEF | polyethylene furanoate |
| PEIS | Potentiostatic Electron Impedance Spectroscopy |
| PET | polyethylene terephthalate |
| ppm | parts per million |
| QTOF | quadruple time of flight |
| TAL | triacetic acid lactone |
| TLC | thin-layer chromatography |
| THF | tetrahydrofuran |
| UV | ultraviolet |

ACKNOWLEDGEMENTS

I am grateful for the opportunity of working under the supervision of Dr. George Kraus. There have been many times I feel challenged conducting research in his lab, but with his motivation and passion for mentoring I was able to comprehend. I will always appreciate his patience and understanding. His dedication and excellence in synthetic organic chemistry will always serve as an inspiration.

I would like to express my gratitude to my graduate committee members: Dr. Brent Shanks and Dr. Arthur Winter for their time and support throughout my stay in Iowa State University. Their opinions and advices were greatly appreciated. I acknowledge Dr. Wenzhen Li, his student Yang Qiu, and the rest of present Li's group members for the opportunity to work in the field of electrochemistry. I would also like to recognize Dr. Wenyu Huang and his group for providing me the experience working in the field of catalysis during the first two semesters of my graduate studies. The computational efforts of Logan Fischer and Shinae Kim were also appreciated.

I feel delighted working in Kraus lab in the presence of my motivating colleagues: Dr. Uma Wanninayake, Dr. Pengfei Dong, Yang Qu, Ivan Geraskin, and Huangchao Yu. Their motivation and support towards the completion of my Masters of Science study were very much highly appreciated. All the intellectual and personal life discussions will always be cherished.

I would especially thank Aaron Zoellner for the great brotherhood he has imparted me. Through my ups and downs in the past year, he has been there to celebrate with and an anchor providing me with great advices and motivation. His unconditional friendship

will always be treasured. I also want to express my heartfelt appreciation to Dr. Michelle Thompson, Hannah Crotty, and Miles Arthur White for all the motivation, suggestions, and advices they have provided me about research and personal struggles. They have always made themselves available if I need them the most. I am also grateful to Fritzie Rivas, Dr. Kristin Manibog, Mapi Faylon, Katrina Lutap, and Darlene Sanchez for bestowing me with their sisterly-love since I moved in to Ames. The companionship of Eric Schultz, Fitim Kelmendi, Peter Spurgeon, Ming-Hsun Cheng, Charles Nyamekye, and Frank Hanes were also greatly acknowledged.

Finally, I would want to express my heartfelt thanks and dedication of this success to my parents Joy and Rey Romal for their sacrifices and unconditional love they have given me my entire life. They have not only provided me with the necessities of life, but they also have endowed me with the luxury of it. They have nurtured me to be resilient, hardworking, and patient. I would also want to dedicate this work to my extended family that have always shown me their love and support towards my graduate studies.

ABSTRACT

Our society has relied mostly on fossil-based materials as source of carbon for industrially important chemicals. The non-renewability of this petroleum-based material, however, requires an alternative for sustainability. Presently, there has already been great advancement in utilizing biomass as a renewable carbon source. Triacetic acid lactone (TAL) has been explored as a potential renewable platform chemical by the Center for Biorenewable Chemicals (CBiRC). In the presence of microbial and enzymatic biocatalysts, TAL can be biosynthesized from glucose. Subsequently, TAL can be transformed to variety of high-valued commodity chemicals using chemical catalysts.

In Chapter 1 of this work, an efficient method was developed to utilize TAL in the 3-components Mannich reaction. This multi-component reaction is an efficient way of making highly-functionalized molecules. The participation of TAL as the enolizable component in the Mannich reaction has not been well studied in the literature. The successful production of Mannich bases containing TAL moiety demonstrates the versatility of TAL as a platform chemical.

In Chapter 2, the corrosion inhibition activity of 2-pyrones, pyridines, and TAL-derived Mannich bases in mild steel was evaluated. There already exist organic molecules corrosion inhibitors. Some TAL-based molecules and pyridines, however, have not been very well known for this application. This chapter gives an overview of other potential small organic molecule corrosion inhibitors. Structure similarity with the previously studied, *opuntiol*, is the basis for evaluating the efficiency of these molecules. Further studies are still needed to compare the activity of these organic molecules with the corrosion inhibitors used in the industry.

~ To God be the glory ~

CHAPTER I

MANNICH REACTIONS OF THE BIO-BASED TRIACETIC ACID LACTONE

1.1 Introduction

1.1.1 Progress to bio-based platform chemicals

Presently, numerous industries from plastics, textiles, and cosmetics, to polymers, pharmaceuticals, and fuel rely on petroleum-based chemicals as one of the raw materials for production. The gradual depletion of fossil-based resources poses a concern to these chemical industries. In addition to this, the risk in coal mining and the generation of environmentally harmful by-products are also factors to seek an alternative for the production of energy. As a result, several efforts have been made to resolve this issue. Many believe that the most feasible solution is to utilize bio-based platform chemicals for sustainability.

The major feedstock for producing bio-based platform chemicals is natural biomass. This may include components such as cellulose, hemicellulose, lignin, and others, in Figure 1, depending on the plant source.^{[1],[2]} The carbohydrate source, however, should be non-edible, a waste material from agricultural processing, or even food waste to avoid competition with the food sector.^[3] Also, the carbohydrate source must be abundant and renewable to attain sustainability of the approach. In 2010, Bond and co-workers reported that the United States increase the production of dry biomass from crops and forest wastes

at 1.3 billion tons per year.^[4] Thus, it is practical to exploit biomass for bio-based platform chemicals production.

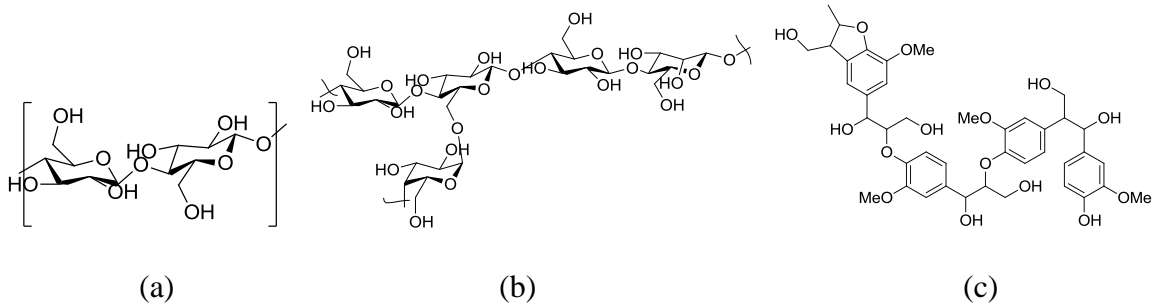


Figure 1: Major components of lignocellulosic biomass. (a) Cellulose, (b) Hemicellulose, and (c) Lignin

Furthermore, the U.S. Department of Energy has identified chemicals that can be derived from biomass, which may be further transformed into other industrially-important chemicals. Initially, the U.S. Department of Energy announced the Top 12 Value Added Chemicals derived from Biomass, but current technological advances in biorefineries shortened the list of marketable bio-based chemicals to top 10 as illustrated in Figure 2.^{[5a],[6]} Two of the criteria of a Top Value Added Chemical, as reported by Bozell and co-workers, is that the compound must display high versatility as a platform that can be functionalized. The compound and its transformation must also be relevant and applicable to large-scale process and production.^[6] For example, 2,5-furandicarboxylic acid (FDCA), satisfies the two criteria mentioned above.

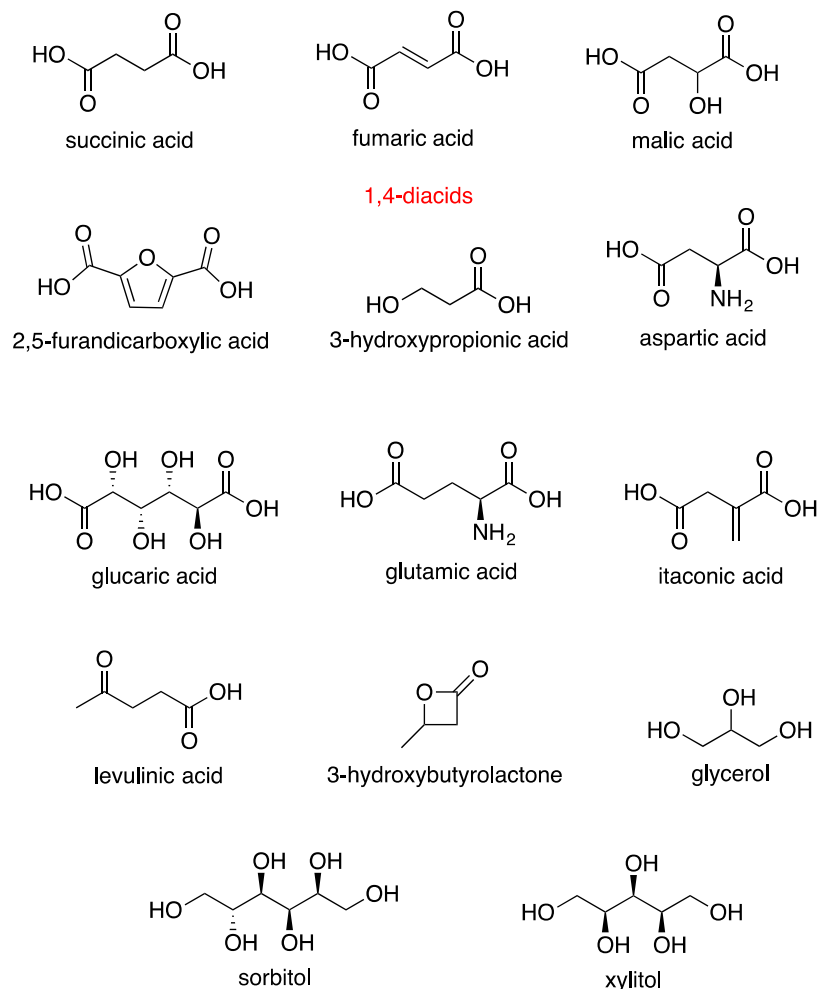
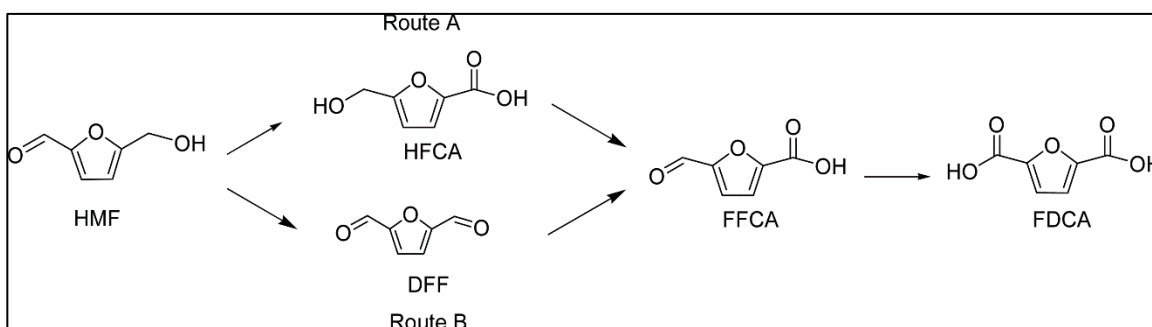


Figure 2: DOE Top Value Added Chemical from Carbohydrates as of 2004

To illustrate the criteria further, FDCA is a derivative of 5-hydroxymethylfurfural (HMF), a dehydration product of fructose or glucose, which can be attained from three consecutive oxidations of HMF as shown in Scheme 1.^[7] The interest in FDCA originates from its potential to replace petroleum-derived terephthalic acid in the big-scale production of various polymers, by the addition of either diol or diamine to initiate the polymerization reaction.^{[6],[8],[9]} Some FDCA-derived compounds have been found to be intermediates in organic synthesis, while some exhibit anti-bacterial or anti-viral activities.^{[10],[11]} To emphasize the practical application of FDCA, it is noteworthy to mention literature reports

that evaluate FDCA-based biopolymers (PEF) as a potential replacement for the petroleum-based polymers (PET). PET is utilized in making soda bottles, as well as in manufacturing fibers for textiles and carpets, to name a few.^[12] The main problem with this technology is the use of terephthalic acid as one of the raw materials, together with ethylene glycol (EG). Although EG has already been produced using bioethanol, the terephthalic acid is not 100% renewable.



Scheme 1: Route of FDCA production from HMF^[7]

Compared to PET, PEF has gained more attention recently from a sustainability standpoint. PEF is synthesized by condensation of FDCA and EG. Both starting materials are renewable chemicals, which make the production of this class of biopolymer 100% renewable. Research reports and patent applications, such as the works of Whinfield, Hachihama, Moore, and Kato and co-workers established the fact the PEF has been extensively evaluated.^{[13]-[16]} However, only recently has PEF's relevance been recognized, due to the current state-of-the-art technology made available. It was reported in 2012 that PEF can compete with PET in terms of price, performance, and sustainability.^[12] De Jong and co-workers claimed that the permeability of H₂O and CO₂ in PEF-based plastic bottles is two times lower than the traditional PET-based plastic bottles. The barrier for O₂ for PEF-based material is asserted to be 6 times higher than the PET-based materials. PEF-

based plastic bottle also preserves its mechanical and physical properties when subjected to stresses during the recycling process.

Notwithstanding the relevance of FDCA, there are still concerns about the industrial production of FDCA from HMF. Although current methods have been developed for this reaction that resulted in both high conversion of HMF and decent selectivity to FDCA, there are still challenges for this conversion. These challenges include the harsh reaction conditions, production of by-products, and FDCA isolation, which pose concerns in industrial-scale production.^{[17]-[19]} These make the production of FDCA from HMF less desirable in biorefineries and others industries alike. The rapid development of current technology in the area of catalysis, including the incorporation of enzyme and heterogeneous catalysis, strive to surpass the limitations presented for mass production of HMF to FDCA.^{[20],[21]}

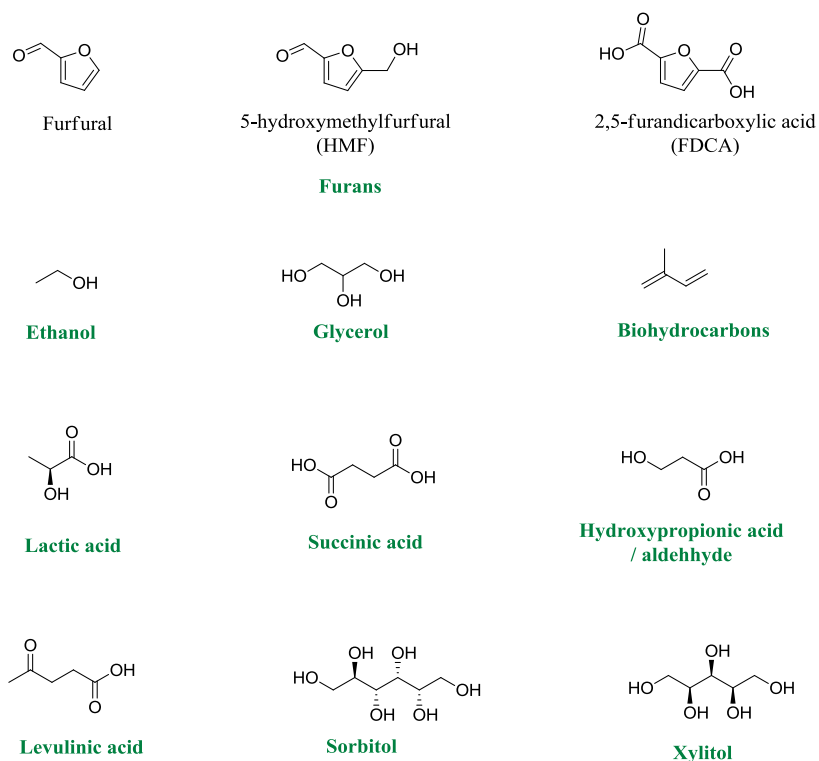
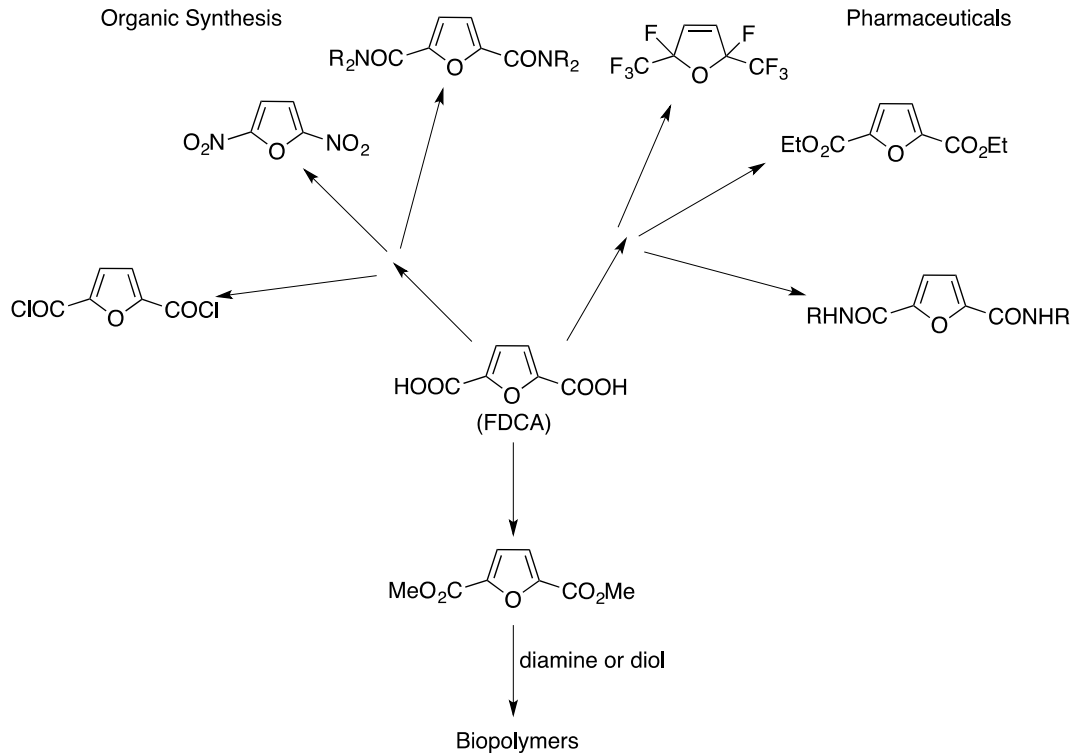


Figure 3: Top 10 Top Value Chemical derived from Biomass^[5b]



Scheme 2: Utilizing FDCA as a platform chemical and as an intermediate of biopolymers

The production of platform chemicals from plant-based carbohydrates provides a remedy to resolve concerns in the depletion of petroleum as a carbon source. As illustrated above, materials composed of bio-based platform chemicals are capable of competing with the petroleum-based materials in terms of performance and economic considerations. If utilization of these neutral carbon sources for the production of platform chemicals advances, the manufacturing process will achieve a high level of sustainability.

1.1.2 Natural products and 2-Pyrone subunit

In addition to the bio-based platform chemicals established by U.S. DOE, there are also other compounds as shown in Figure 4. Raw biological materials, from roots, leaves, and barks, to fruits and seeds, contain natural products that are well known to be actively

used as medicines.^[22] For example, analgesics composed of acetylsalicylic acid derived from the natural product salicylic acid (Figure 4) found in willow bark is one of the most popular. In the Republic of Philippines, *Blumea balsamifera* (Alibum), *Lagerstroemia speciosa* (Banaba), and *Coleus aromaticus* (Oregano) are common multi-purpose herbal plants that contain L-(-)-camphor, corrosolic acid, and protocatechuic acid ester derivatives, respectively, (Figure 4).^{[23]-[25]} These compounds act as active ingredients to combat inflammation and bacterial infection. However, only a few milligrams per kilogram of these ingredients are actually harvestable from each plant.^[26] One way to enhance the amount of these biologically-active materials produced in plants is to incorporate genetic engineering of microorganisms, such as *Escherichia coli* (*E. coli*). The challenge for this technology, is that fermentation process is not very practical for large-scale production. As a result, other techniques for the production of natural products such as organic synthesis should be considered.

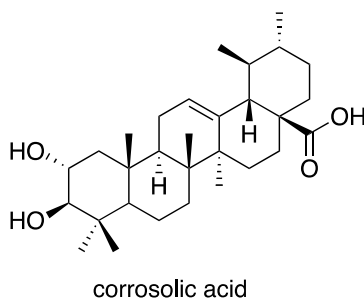
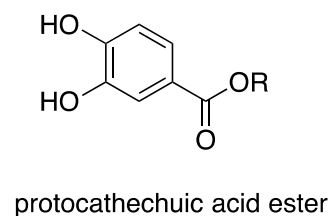
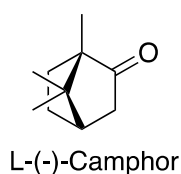


Figure 4: Natural products used for medicinal purposes

In addition to the wide variety of compounds present in natural products, pyrones have been found as one of the most abundant in many biological materials. The pyrone subunit is a cyclic ester and is known for its high pharmaceutical activity, especially 2-pyrone. Figure 5 shows a selection of natural products containing 2-pyrone.^[27] Achrocarpin E is reported to show cytotoxic activities towards the A2780 ovarian cancer line.^[28] Bufalin is found to be an efficient inhibitor of the p160 steroid receptor coactivator family, which^[29] plays a role in many type of cancers by protein degradation and blockage of cancer cell growth at low concentrations. Additionally, Herbarin A is an active antioxidant and Pyripyropene A exhibits activity as a coenzyme acyl-CoA:cholesterol acyltransferase (ACAT) inhibitor.^[27] This type of inhibitor can potentially be used in the treatment of hypercholesterolemia and atherosclerosis.^[30]

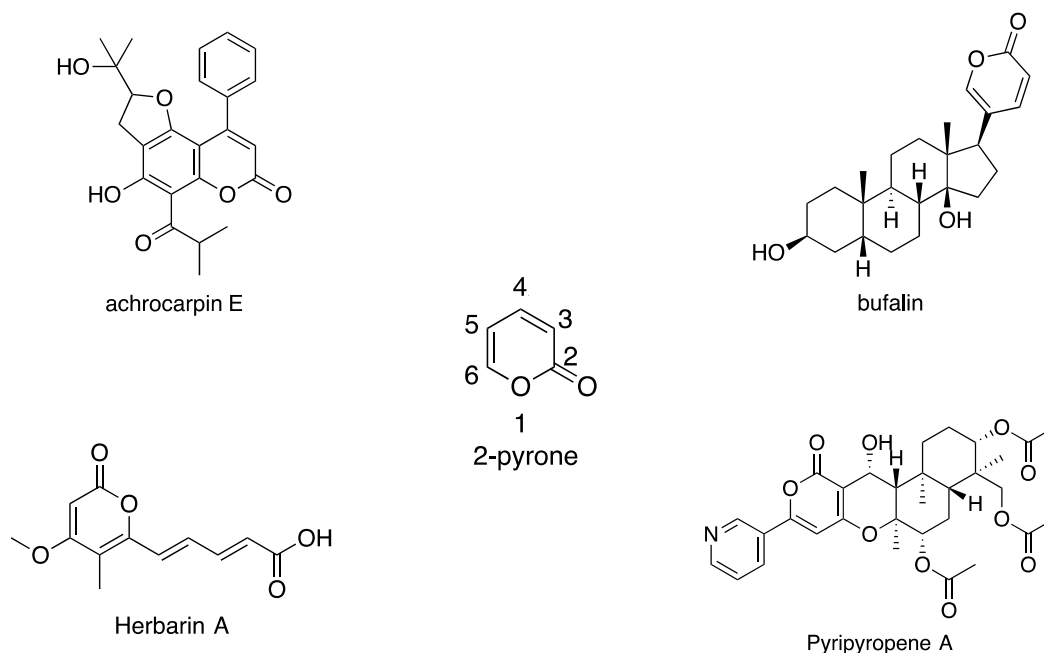
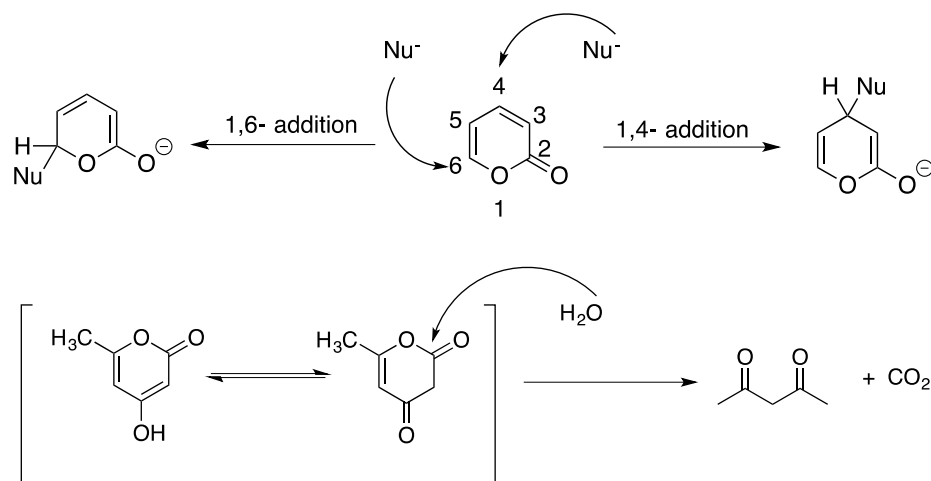


Figure 5: 2-pyrone and natural products containing 2-pyrone subunit

As mentioned above, the amount of these natural products extracted from its biological material sources is currently very low. The application of metabolic engineering to increase natural production of these biological compounds is hindered by the inefficient fermentation step. To further study the potential cytotoxic, phytotoxic, and neurotoxic properties of natural products, larger quantities are required. To increase the amount of production of these natural products, synthesis from smaller molecules followed by functionalization should be explored. One approach is to start with the readily available 2-pyrones. This subunit is a key intermediate in biosynthetic processes that is easily metabolized.^[31]

Also, 2-pyrones are found in many microorganisms such as bacteria and microbes.^[32] This compound has been reported to act as a defense mechanism agent against other inhibiting organisms, animals, and insects. This also plays a vital role as a biosynthetic intermediate and as a metabolite. The pharmaceutical activities of 2-pyrone subunit make it an interesting unit to be considered for functionalizing. Furthermore, the reactivity of 2-pyrone subunit varies at each atom position of the ring system. Moreno-Mañas and co-workers explained that for 2-pyrones, position 3 and 5 are nucleophilic in nature; positions 2, 4, and 6 are electrophilic as shown in Scheme 3.^[33] Nucleophilic attack at position 2 may cause a ring opening of the 2-pyrone as studied with triacetic acid lactone (TAL) by Chia and co-workers, shown in Scheme 3.^[34] In addition, nucleophilicity of 2-pyrone is observed in nitration, sulfonation, and halogenation reactions, which displays its aromatic nature.^[35] The reaction of 2-pyrone as a diene with a dienophile in Diels-Alder reactions demonstrates its unsaturated aliphatic character.^[36] The presence of substituents on the 2-pyrone ring, furthermore, enhances favorable interactions for example, the

presence of electron-donating groups at C-4 and C-6 facilitates electrophilic attack on the ring.^[5b] Electron-withdrawing groups at C-3 initiates nucleophilic substitutions at C-4 and C-6, where 1,6-addition product is more favored than 1,4-addition product. If, however, C-4 contains a leaving group, then C-4 is more favored for nucleophilic attack than C-6.



Scheme 3: Nucleophilic substitutions of 2-pyrone

As discussed, the 2-pyrone moiety is a versatile unit that can undergo aromatic substitutions and olefinic reactions, such as Diels-Alder reaction. The reactivity of this ring system offers routes for the synthesis of a variety of natural products and analogs. This also can gain access to related materials. Furthermore, two simple naturally-occurring substituted 2-pyrones: 4-hydroxy-6-methyl-2-pyrone (TAL) and 3-acetyl-4-hydroxy-6-methyl-2-pyrone (dehydroacetic acid, DHA), shown in Figure 6, are biosynthesized from acetic acid. These molecules have exhibited potential as platform chemicals for the synthesis of many complex molecules.

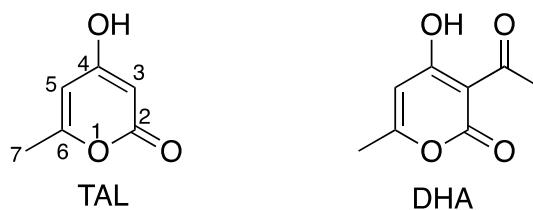
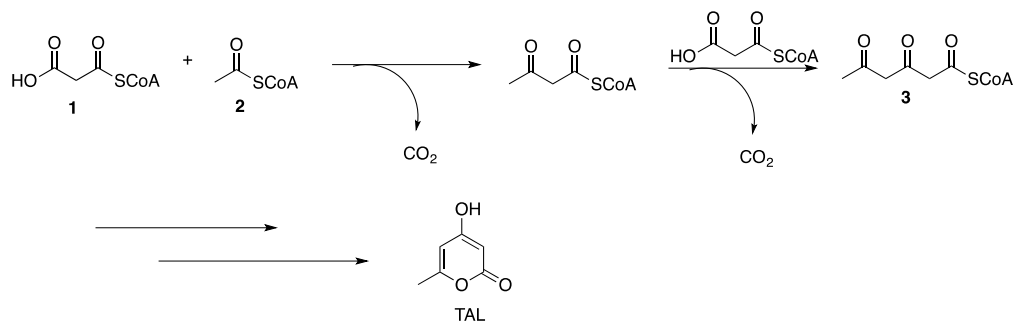


Figure 6: Naturally-occurring simple 2-pyrones

1.1.3 Biobased triacetic acid lactone and its reactivity

Triacetic acid lactone has been studied by the Center for Biorenewable Chemicals (CBiRC). One of the ways TAL is achieved is through the polyketide biosynthesis as the major triketide derailment product.^{[37],[38]} This biological pathway of TAL synthesis from glucose is catalyzed by the bi-functional enzyme 2-pyrone synthase (2-PS), a Type III polyketide synthase *g2ps1* isolated from *Gerbera hybrid*, as shown in Scheme 4a. This contains a specific protein that plays a crucial role of decarboxylating malonyl coenzyme A (malonyl CoA, **1**) to acetyl coenzyme A (acetyl CoA, **2**), in the absence of **2**.^[39] Also, this catalyzes condensation of one molecule of **2** and two molecules of **1** to form the polyketide chain **3**. The same enzyme that promoted decarboxylation and condensation also enforces ring closure of **3** by deprotonation followed by intermolecular nucleophilic attack to form TAL.^[26]



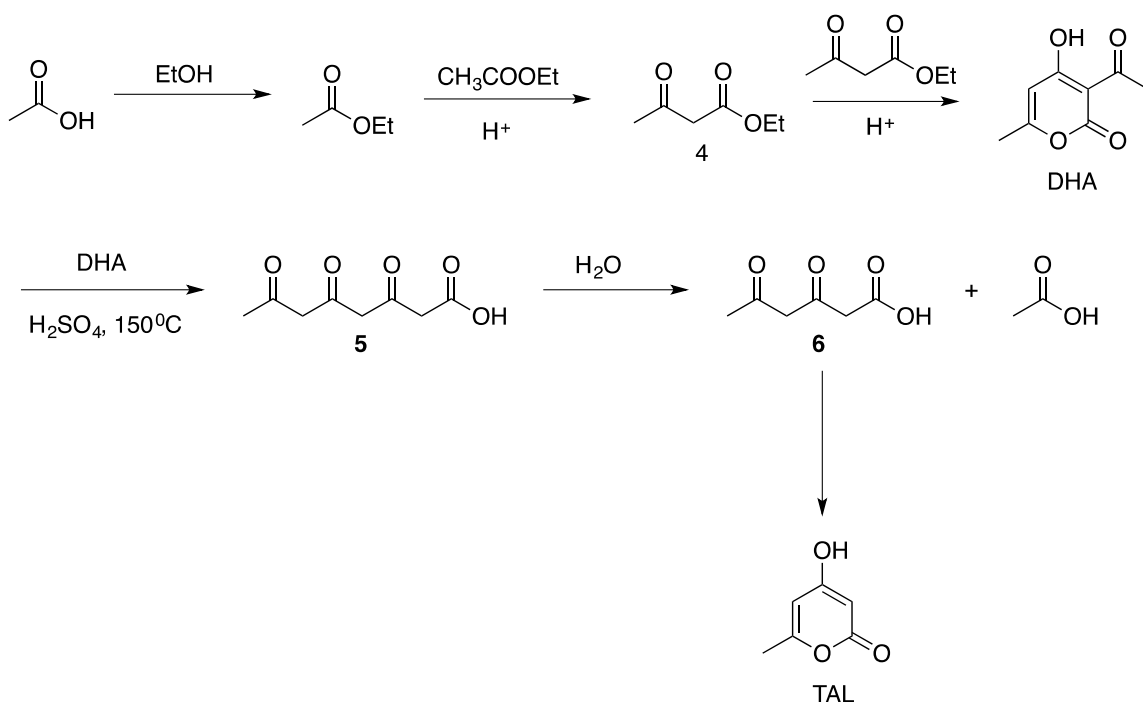
Scheme 4a: Proposed biosynthetic pathway to the production of TAL^[37]

Current progress in microbial and metabolic engineering has opened an opportunity for the industrial biosynthesis of TAL. In 2006, Xie and co-workers published the highest TAL titers reported from using wild-type 2-PS expressed in *E. coli* and from incorporating *Saccharomyces cerevisiae* at 0.47 g/L and 1.8 g/L, respectively.^[39] Cardenas and Da Silva advanced the production of TAL via metabolically-engineered 2-PS enzyme expressed in *E. coli* at 2.1 g/L, while TAL titer of using 2.2 g/L was claimed using *Saccharomyces cerevisiae* strain BY4741 in 2013 and 2014, respectively.^{[37],[40]} Recently, Saunders and co-workers have developed a technique that does not require metabolic engineering of microbes, but rather the transformation of 2-pyrone synthase (*g2ps1*) to 13 industrial yeast strains containing different genetic information.^[41] This method produces 5.2 g/L TAL titer, the highest biosynthesized TAL attained. Despite not integrating metabolic engineering in their recent work, Saunders and co-workers expressed interest in engineering the strains to improve the yield of TAL from metabolic process.

Currently, TAL is manufactured through chemical synthesis. Industrial production of TAL is attained through commercially available DHA. DHA is processed from acetic acid via esterification, condensation, and ring closure. Scheme 4b shows the total synthesis of TAL from DHA. The synthesis of TAL starts with the esterification of AcOH with EtOH to form EA.^{[41]-[43]} Then, two molecules of EA react via Claisen condensation to form **4**, followed by self-Claisen condensation, then ring closure to obtain DHA. In the presence of H₂SO₄, DHA undergoes ring opening to **5**, deacylation to **6**, then, eventually ring closure to obtain TAL.

Owing its physical and chemical properties to the 2-pyrone moiety, TAL is known to be reactive towards many transformations. As with 2-pyrone in Figure 5, C-3, C-5, and

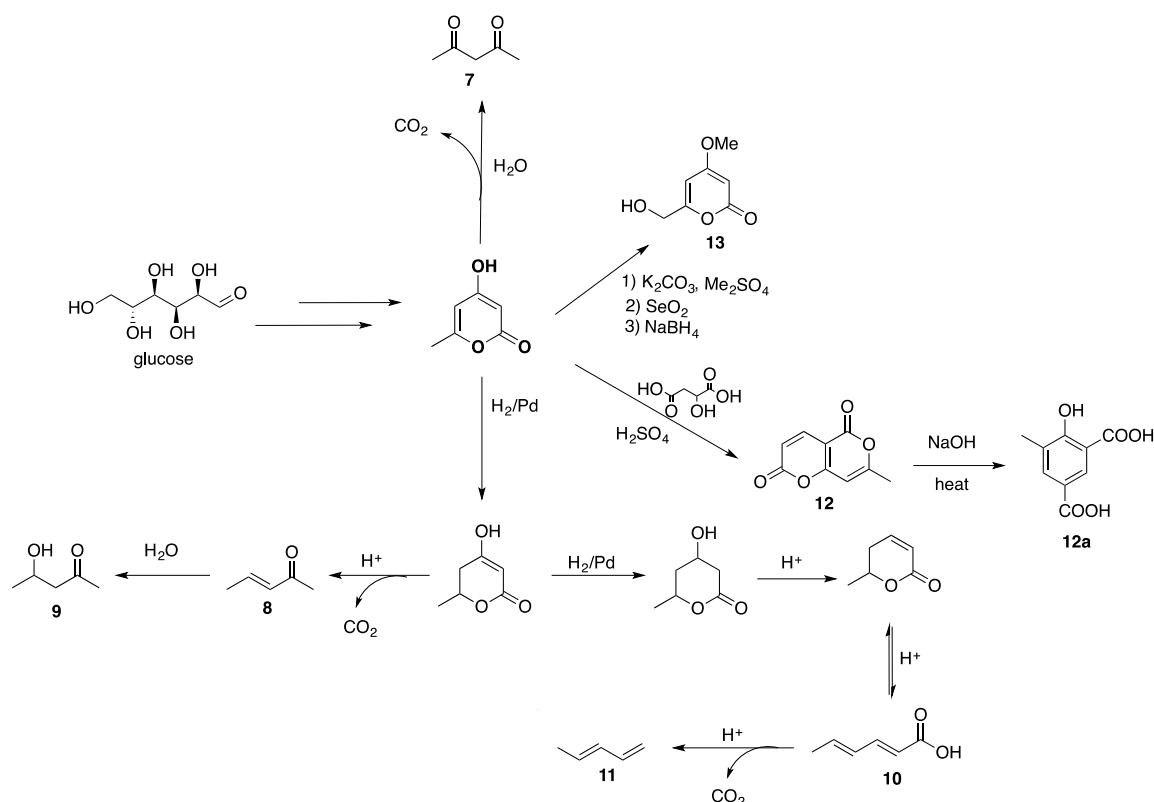
C-7 are nucleophilic, while C-2, C-4, and C-6 are electrophilic. Scheme 5 and Scheme 6 illustrate the versatility of TAL as a platform chemical. TAL can be transformed into wide network of relevant derivatives and complex molecules that can be considered as high-valued chemicals or those that have high biological activities. Scheme 5 shows the chemical transformations from TAL reported in the literature, while Scheme 6 shows TAL functionalized compounds synthesized in our lab.



Scheme 4b: Total synthesis of TAL from AcOH

To briefly discuss the importance of these TAL-derived molecules, compound **7** in Scheme 5 is a precursor to a commonly used bidentate ligand, acetylacetonate, as well as for the production of heterocyclic compounds.^{[5b],[34],[44]-[47]} Compound **8** is used as a solvent for coatings and industrial cleaning, while sorbic acid (**10**) is utilized as a food preservative to prevent growth of fungi and molds. Sorbic acid can then be decarboxylated in the presence of an acid to form diene **11**, known industrially as piperylene, which is used

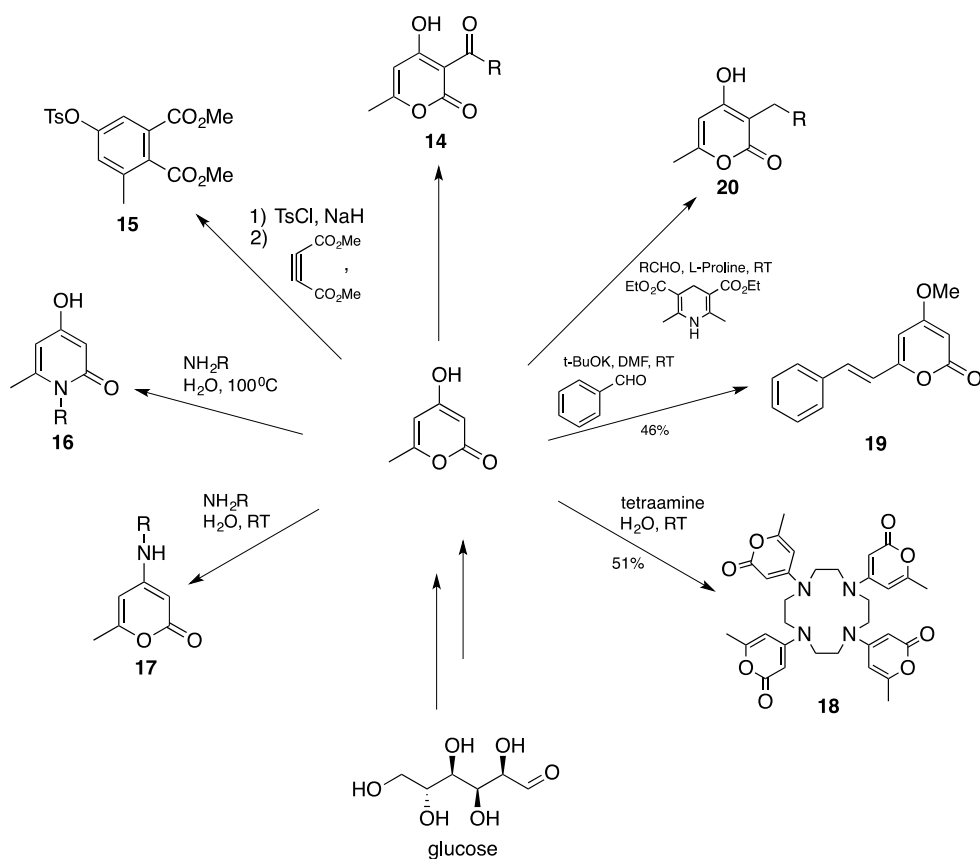
as monomer for plastics and adhesives. Bicyclic compound **12** can be transformed to **12a**, a derivative of salicylic acid that may have the similar anti-bacterial activity as its parent compound. Moreover, compound **13**, *opuntiol*, can be obtained TAL *via* three-steps and has shown anti-corrosion activity in mild steel under acidic conditions.



Scheme 5: TAL derivatives reported in literature

Scheme 6 shows the synthesis of several TAL derivatives, based on methods developed in our group. Compound **14**, pogostone, and its derivatives, are reported to have activity against yeast-like organisms and are obtained at a very good yield from TAL.^[5b] Also, TAL reacts with DMAD *via* a Diels-Alder reaction to produce **15**, which is a carboxylic ester derivative of phthalic acid. Compounds **16** and **17**, which have high pharmaceutical potential, are synthesized by the addition of a primary amine in H₂O.^[48] It

has been determined that compound **16** is the thermodynamic product, while compound **17** is the kinetic product. Interestingly, a relatively new idea for application of TAL derivative is metal chelation for metal detection and wastewater treatment of **18**, which is currently under study.^[5b] Finally, compounds **19** and **20** are also synthesized from TAL. They were reported to have demonstrated pharmaceutical activities.^{[49],[50]}



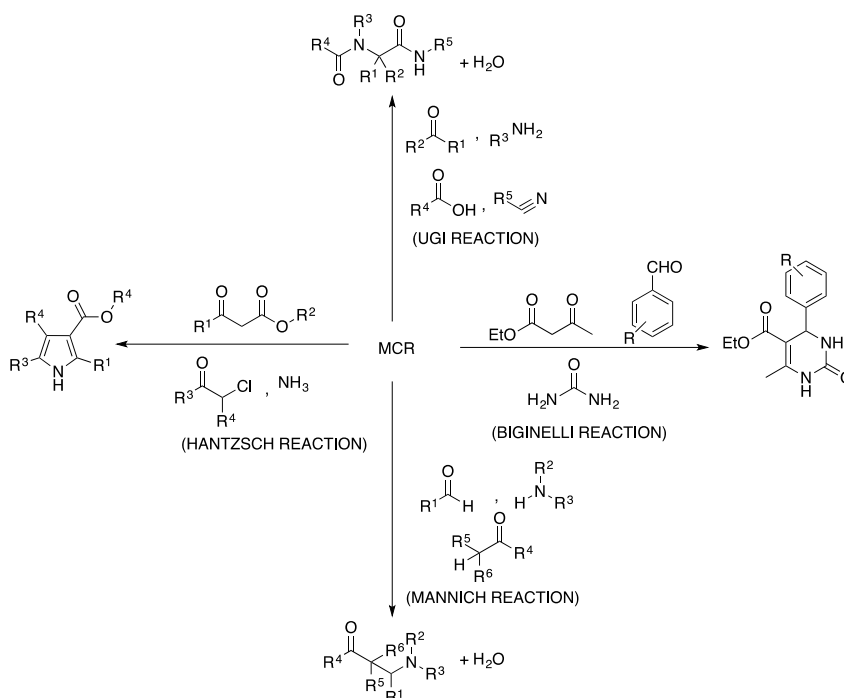
Scheme 6: TAL derivatives synthesized from Kraus' group

1.1.4 Mannich reaction as a route to molecular diversification

As discussed above, natural products can be synthesized from versatile platform chemicals. Once a potential platform chemical has shown promise for functionalization,

synthesis of complex molecules from a simple substrate can be attained. Similarly, the route to molecular diversity applies this approach.

Multicomponent reactions (MCRs) are known methods to expand the library of molecular complexity and diversity.^[51] MCR products have attracted the attention of biologists and medicinal scientists due their predefined functionalities.^{[52]-[54]} Not only that, but MCRs provide processes that are efficient, have a low cost of operation, and exhibit superior atom economy.^[55] In these reactions, several bond breaking and bond forming events occur that eventually lead to a stable product. One of the most important bond formations in synthetic organic chemistry is the C-C bond formation. There are several known multicomponent reactions that initiate C-C bond formations such as Ugi, Biginelli, Hantzsch, and Mannich reactions, as shown in Scheme 7. In the current study, molecular diversification is expanded via the Mannich reaction to utilize the bio-based TAL producing three-component products.



Scheme 7: Selected multicomponent reactions

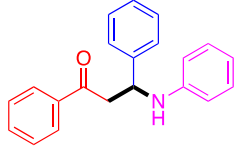
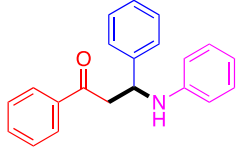
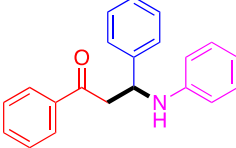
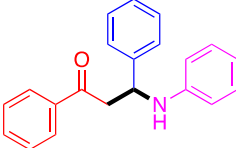
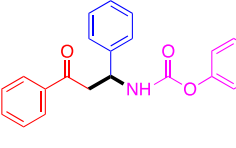
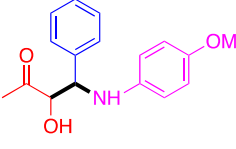
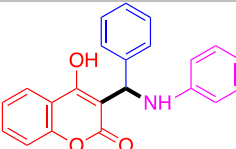
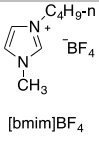
The Mannich reaction is a three-component reaction consisting of an amine, aldehyde, and a ketone with an active α -hydrogen. The product, called a Mannich base, is a β -amino carbonyl compound bearing nitrogen moiety. The nitrogen moiety provides improvement of its physicochemical properties, like water solubility.^[56] As a result, this enhances the bioactivity of Mannich bases towards pharmaceutical applications.^[57] Not only does the nitrogen group cause its compatibility for pharmaceutical applications, but it also plays a role as an active species for corrosion inhibition in mild steel.^{[58]-[60]}

The literature has wide arrays of synthetic methods for the production of Mannich bases in one-pot reactions. As claimed by Wang and co-workers, the reaction of acetophenone, benzaldehyde, and aniline at RT for 30 hours was unsuccessful,^[61] which illustrates that a catalyst could be necessary for the Mannich reaction to occur. Several catalysts have been reported to produce the Mannich bases of acetophenone, benzaldehyde, and aniline in very high yield as shown in Table 1.^{[62]-[66]} The polymer-supported sulfonic acid (PS-SO₃H) in H₂O has shown activity in the Mannich reaction. The transition metal salt NbCl₅ is more active than PS-SO₃H. The lanthanide salt ((NH₄)₂Ce(NO₃)₆) in PEG yields the product at shorter time at higher temperature than using NbCl₅ in EtOH. Finally, copper nanoparticles (CuNP) provide the best efficiency for this reaction system. Furthermore, Entries 6 and 7 in Table 1 show that in the presence of α -hydroxy group, the α -hydrogen to the hydroxyl and ketone is deprotonated. This is due to the stability of carbanion formed by keto-enol tautomerization of the two oxygen-bearing functional groups.

Despite the high yield of these Mannich bases, however, there are various drawbacks with the current methods. The toxicity of some catalysts, relatively high acidic

condition, and use of 10-20 mol% amount of the catalysts are the major concerns for the current process. Therefore, the development of a method that promotes the use of benign catalyst and in lower amounts is crucial. Once an improved method is developed, the route to molecular complexity and diversity by Mannich reaction will be highly accessible.

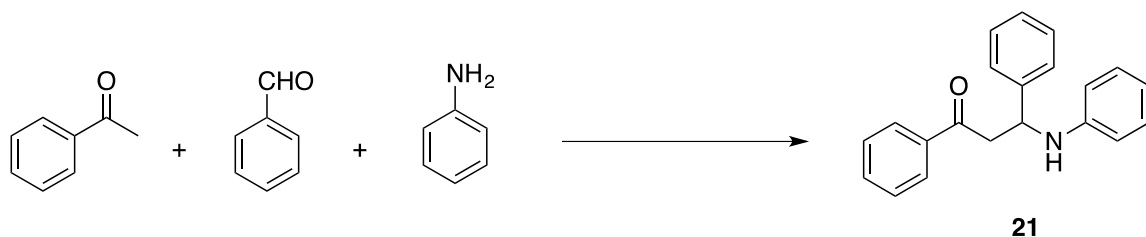
Table 1: Literature methods for 3-components Mannich reaction^{[62]-[66]}

| ENTRY | PRODUCT | CATALYST | SOLVENT | TIME (hr) | T (°C) | % Yield |
|-------|---|--|------------------|-----------|-----------------------|---------|
| 1 |  | NbCl ₅ | EtOH | 12 | RT | 95 |
| 2 |  | PS-SO ₃ H | H ₂ O | 24 | 30 | 75 |
| 3 |  | CuNP | MeOH | 8 | RT | 93 |
| 4 |  | (NH ₄) ₂ Ce(NO ₃) ₆ | PEG | 9 | 45 | 98 |
| 5 |  | I ₂ | MeCN | 24 | RT | 78 |
| 6 |  | L-Proline | DMSO | 1 | Microwave irradiation | 90 |
| 7 |  |  [bmim]BF ₄ | neat | 8 | RT | 74 |

1.2 Results and Discussion

Literature reports on Mannich bases have shown their applications in pharmaceutical industries for their cytotoxic, phytotoxic, and neurotoxic activities. In addition to these efforts in pharmaceutical research, a recent advancement applies Mannich bases as potential corrosion inhibitors in different metals. In this report, the goal is to develop a novel method for the synthesis of 3-component Mannich bases-containing TAL moiety in a one-pot reaction. Efficient methods for this process will result in high accessibility to diverse and well-functionalized molecules.

Table 1 above shows several reports that use variety of catalysts in different solvents for the reaction in Scheme 8. Most catalysts used for this specific reaction are acidic in nature, like Lewis acids and Cu NP, which are known to be slightly acidic. Also, these catalysts were used between 10 to 20 mol%. To improve cost efficiency and avoid a harsh reaction environment, it was proposed that AcOH (1 mol%) should be used as the catalyst. To confirm the activity of AcOH in Mannich reactions, the reaction in Scheme 8 was run with AcOH as the catalyst, as well as with a variety of solvents. As shown in Table 2, the reaction was successful in all solvents screened. The formation of the Mannich base was confirmed *via* TLC and LRMS. This result illustrates that AcOH is a compatible catalyst for Mannich reactions. Also, since dimethoxymethane (DMM) has been found to work well during the preliminary studies of the Mannich reactions of TAL, it was chosen as an appropriate solvent for this system.

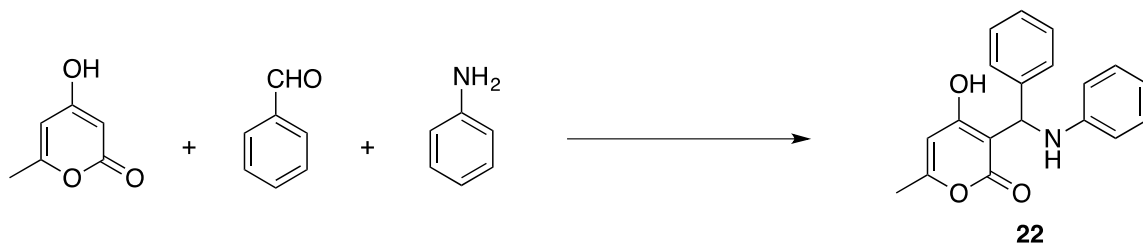


Scheme 8: Mannich reaction of acetophenone, benzaldehyde, and aniline

Table 2: Testing the activity of AcOH as catalyst in Mannich reaction. Reaction conditions: acetophenone (1.0 mmol), benzaldehyde (1.0 mmol), aniline (1.0 mmol), AcOH_(cat.), 24hours, and RT with stirring.

| Solvent | Product |
|---------|-----------|
| EtOH | 21 |
| MeCN | 21 |
| DMM | 21 |

Moreover, to promote efforts on utilizing biorenewable molecules as platform chemical, TAL was used with aldehydes and amines to prepare Mannich bases. In order to examine the reactivity of TAL as the enolizable component, acetophenone in Scheme 8 was replaced with TAL in Scheme 9. Similarly, all solvents screened for the reaction in Scheme 8 also produced the target material **22** in Scheme 9 as shown in Table 3. The presence of Mannich base **22** was confirmed *via* TLC and LRMS.

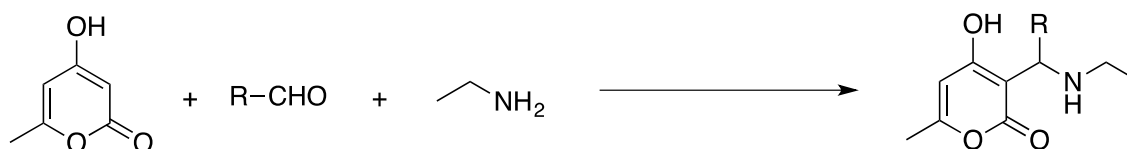


Scheme 9: Mannich reaction of TAL, benzaldehyde, and aniline

Table 3: Testing the reactivity of TAL in Mannich reaction. Reaction conditions: TAL (1.0 mmol), benzaldehyde (1.0 mmol), aniline (1.0 mmol), AcOH_(cat.), 24hours, and RT with stirring.

| Solvent | Product |
|---------|-----------|
| EtOH | 22 |
| MeCN | 22 |
| DMM | 22 |

Extending the effort to efficiently produce well-functionalized Mannich bases containing the TAL moiety, appropriate aldehydes were screened for the reaction in Scheme 10. Results of this Mannich reaction are reported in Table 4. Ethylamine was chosen for this reaction to eliminate the bulkiness of the nucleophile, consequently eliminating steric issues. The reactions were stirred at room temperature for 16-24 hours under air.



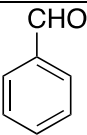
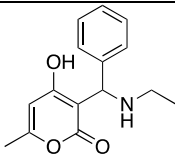
Scheme 10: Mannich reaction of TAL, aldehydes, and ethylamine

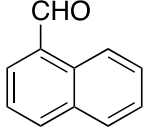
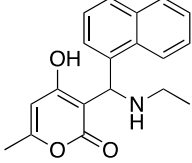
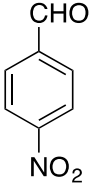
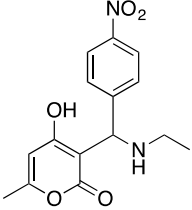
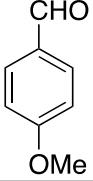
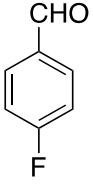
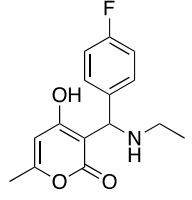
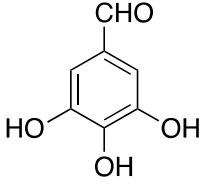
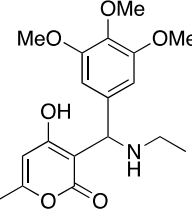
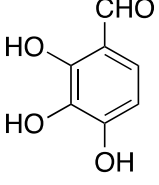
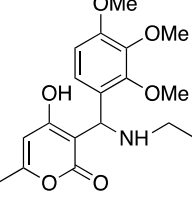
Different aromatic aldehydes were screened to find the most reactive electrophile that produces the highest yield of Mannich base. Without the presence of any stabilizing substituents, **23** was produced as shown in Entry 1 in Table 4. However, due to challenges in purification, it was not isolated. When 1-naphthaldehyde was used, a 32% yield of **24** was obtained. Furthermore, several *para*-substituted benzaldehydes were used as shown in Entries 3-5 in Table 4. For electron-donating groups (EDG), such as methoxy, an increase in the yield compared to Entry 1 was expected. However, *p*-methoxybenzaldehyde did not

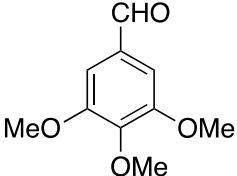
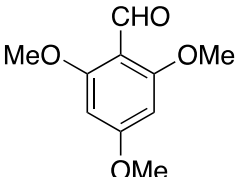
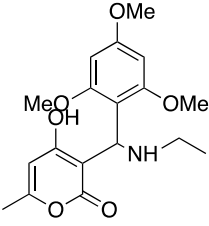
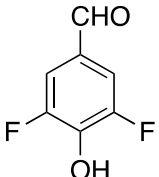
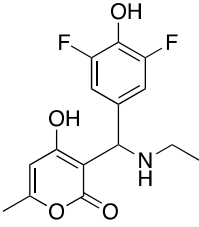
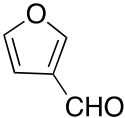
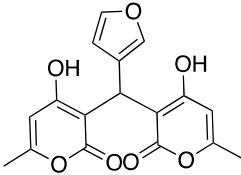
provide its respective product, surprisingly. Meanwhile, an electron-withdrawing group (EWG), such as nitro and fluorine, has shown reactivity for the reaction to obtain **25** and **26**, respectively.

Furthermore, trisubstituted benzaldehydes were also screened in Entries 6-10 in Table 4, which produced Mannich bases between 50% and 60% yield. Surprising results were obtained when Mannich reactions of TAL, ethylamine, and trihydroxybenzaldehyde were employed. Instead of producing Mannich bases containing three hydroxyl groups on the benzene ring, products **27** and **28** containing three methoxy groups were obtained. This suggests that dimethoxymethane acted as a methylating agent for this specific reaction. To further investigate this peculiarity, 3,4,5-trimethoxybenzaldehyde was used as the electrophile. The $^1\text{H-NMR}$ spectrum of the products in Entries 6 and 8 were compared and the shift in signals match exactly. This confirms the production of **27** from the reaction in Entry 6. When furfuraldehyde was used, the bis-Mannich product **31** was obtained in Entry 11. Out of all aldehydes screened, nitrobenzaldehyde has provided the highest yield of the reaction in Scheme 10 at 88%. This shows that *p*-nitrobenzaldehyde is the most reactive aldehyde to employ as the electrophile for the Mannich reaction in the current study.

Table 4: Screening of aldehydes. Reaction conditions: TAL (0.5 mmol), aldehyde (1.0 mmol), ethylamine (0.5 mmol), DMM, AcOH_(cat.), 16 to 24 hours, and RT with stirring.

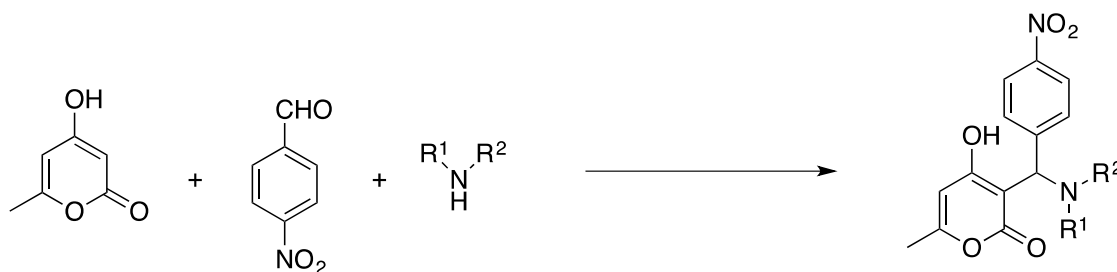
| ENTRY | ALDEHYDE | PRODUCT | % YIELD |
|----------|---|---|---------|
| 1 |  |  23 | ✓ |

| | | | |
|---|---|---|----|
| 2 |  |  <p style="text-align: center;">24</p> | 32 |
| 3 |  |  <p style="text-align: center;">25</p> | 88 |
| 4 |  | X | X |
| 5 |  |  <p style="text-align: center;">26</p> | 11 |
| 6 |  |  <p style="text-align: center;">27</p> | 62 |
| 7 |  |  <p style="text-align: center;">28</p> | 59 |

| | | | |
|----|---|--|----|
| 8 |  | 27 | 55 |
| 9 |  |  | 62 |
| 10 |  |  | 50 |
| 11 |  |  | ✓ |

Using the experimentally established reaction conditions, the Mannich reactions of TAL and *p*-nitrobenzaldehyde with variety of amines were pursued. The use of aliphatic amines, anilines, benzylamines, and cyclic amines as nucleophiles are reported in Tables 5, 6, 7, and 8, respectively. To discuss, when hydrazine was used as the nucleophile, the Mannich reaction was unsuccessful. Using chained primary amines, high yields of Mannich bases were obtained between 75%-80% shown in Entries 2,4, and 5 in Table 5. Secondary amines were also used, Entries 6 and 7 in Table 5. The low reactivity of secondary amine may be due to the steric issues caused by the two R groups. Furthermore,

when allyl amine and diallyl amine were used, Mannich bases **35** and **36** were obtained, respectively. No reaction occurred when diethanolamine and iminodiacetic acid were used.



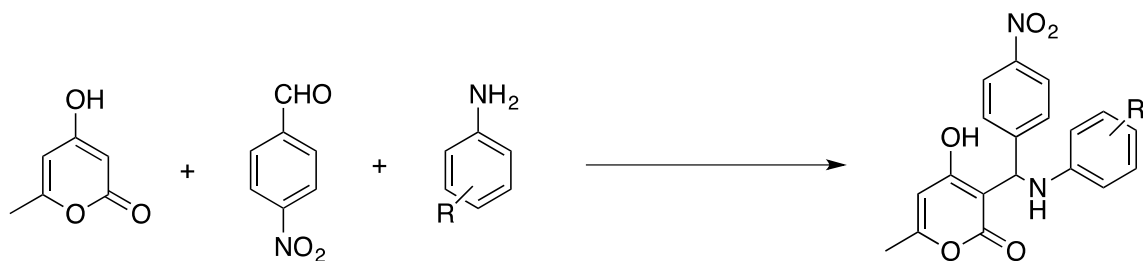
Scheme 11: Mannich reaction of TAL, *p*-nitrobenzaldehyde, and aliphatic amine

Table 5: Mannich reaction of aliphatic amines. Reaction conditions: TAL (1.0 mmol), nitrobenzaldehyde (1.0 mmol), amine (1.0 mmol), DMM, AcOH_(cat.), and RT with stirring.
*Compound **37** was obtained using CH₂Cl₂ as the solvent

| ENTRY | AMINE | TIME (HRS) | PRODUCT | %YIELD |
|----------|--|------------|---------------|--------|
| 1 | H ₂ N-NH ₂ | 16 | X | X |
| 2 | H ₂ N-CH ₂ -CH ₃ | 16 | 25 | 88 |
| 3 | H ₂ N-CH ₂ -COOH | 6 | 37 | ✓ |
| 4 | H ₂ N-CH ₂ -CH ₂ -CH ₂ -CH ₂ -CH ₃ | 16 | 32 | 75 |
| 5 | H ₂ N-CH ₂ -CH ₂ -CH ₂ -CH ₂ -CH ₂ -CH ₂ -CH ₂ -CH ₂ -CH ₃ | 16 | 33 | 84 |

| | | | | |
|----|--|----|---|----|
| 6 | | 16 | | 17 |
| 7 | | 24 | X | X |
| 8 | | 24 | | 60 |
| 9 | | 72 | | ✓ |
| 10 | | 16 | X | X |
| 11 | | 48 | X | X |

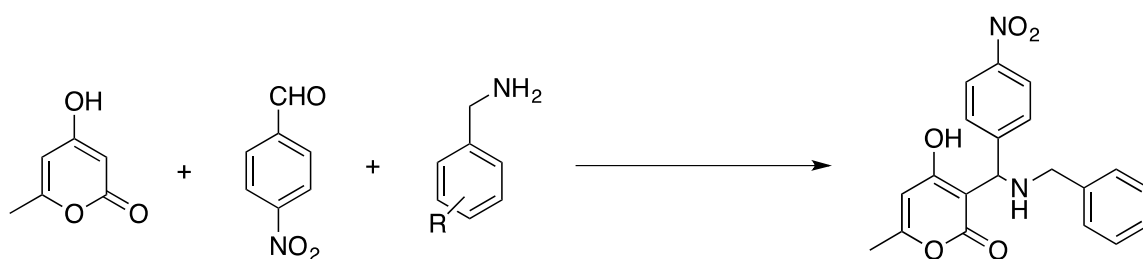
For the Mannich reactions of anilines in Scheme 12, the results are reported in Table 7. The unsubstituted aniline produces its Mannich base **38** at 54% yield in the absence of any stabilizing groups. Halogen-substituted anilines were also used as nucleophiles in Entries 2-6. Out of all these, *o*-bromoaniline showed the highest reactivity producing 62% yield of its Mannich base **40**. When *o*-fluoroaniline was used, only 37% yield of product **41** was obtained, while no reaction occurred when *o*-iodoaniline was used. No reactivity was observed when N-substituted anilines in Entries 7-9 were used as nucleophiles.

Scheme 12: Mannich reaction of TAL, *p*-nitrobenzaldehyde, and anilinesTable 7: Mannich reaction of anilines. Reaction conditions: TAL (0.5 mmol), nitrobenzaldehyde (0.5 mmol), amine (0.5 mmol), DMM, AcOH_(cat.), and RT with stirring.

| ENTRY | AMINE | TIME (HRS) | PRODUCT | % YIELD |
|-------|-------|------------|---------------|---------|
| 1 | | 24 | 38 | 54 |
| 2 | | 24 | 39 | ✓ |
| 3 | | 24 | 40 | 62 |
| 4 | | 48 | X | X |
| 5 | | 24 | 41 | 37 |

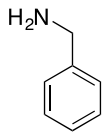
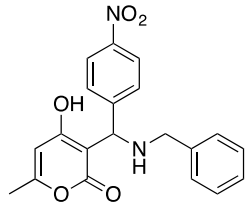
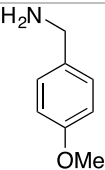
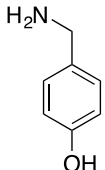
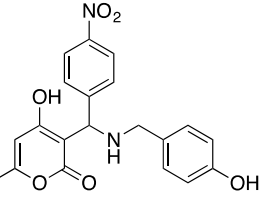
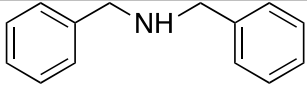
| | | | | |
|---|--|----|---|---|
| 6 | | 24 | X | X |
| 7 | | 48 | X | X |
| 8 | | 72 | X | X |
| 9 | | 24 | X | X |

The results for the reaction in Scheme 13 are reported in Table 8. For benzylamines, the effect of the presence of substituents in the aromatic ring is still inconclusive. While the unreactivity of the reaction in Scheme 3 using dibenzylamine could be due to the steric issues caused by the two phenyl groups.

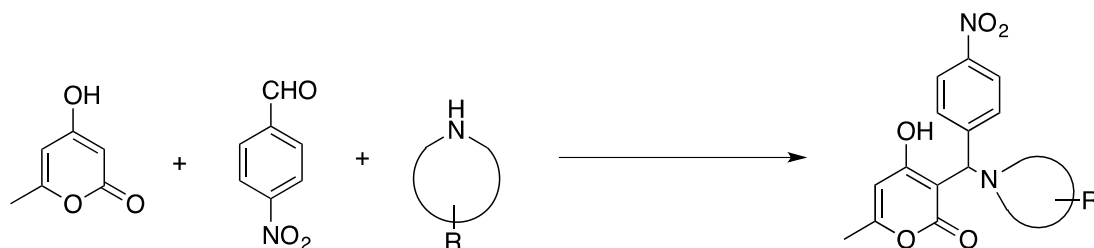


Scheme 13: Mannich reaction of TAL, *p*-nitrobenzaldehyde, and benzylamines

Table 8: Mannich reaction of benzylamines. Reaction conditions: TAL (0.5 mmol), nitrobenzaldehyde (0.5 mmol), amine (0.5 mmol), DMM, AcOH_(cat.), and RT with stirring.

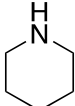
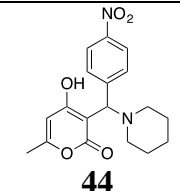
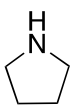
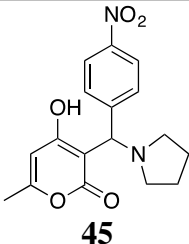
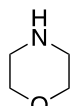
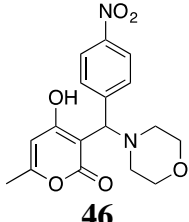
| ENTRY | AMINE | TIME (HRS) | PRODUCT | % YIELD |
|-------|--|------------|--|---------|
| 1 |  | 16 |  42 | 75 |
| 2 |  | 72 | X | X |
| 3 |  | 48 |  43 | 72 |
| 4 |  | 24 | X | X |

The results of the reaction in Scheme 14 are reported in Table 9. Using cyclic amines as nucleophiles, the yields of their respective Mannich bases were consistently between 65-70%. Also with the Mannich reaction with cyclic amines, high ease of isolation of the pure product was achieved.

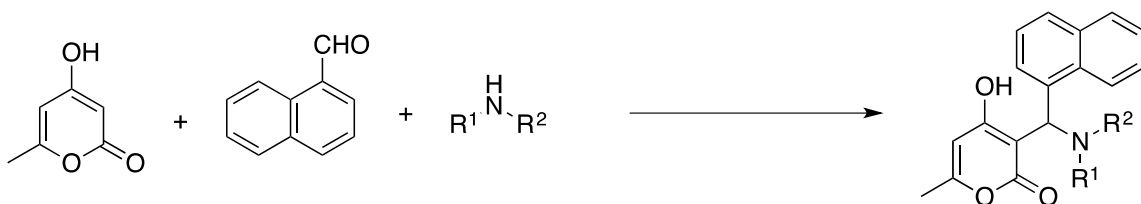


Scheme 14: Mannich reaction of TAL, *p*-nitrobenzaldehyde, and cyclic amines

Table 9: Mannich reaction of cyclic amines. Reaction conditions: TAL (0.5 mmol), nitrobenzaldehyde (0.5 mmol), amine (0.5 mmol), DMM, AcOH_(cat.), and RT with stirring.

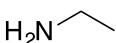
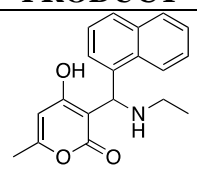
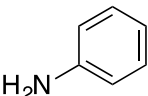
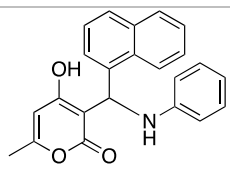
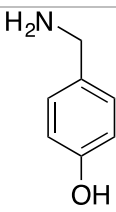
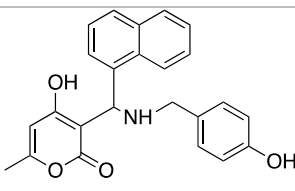
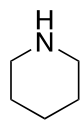
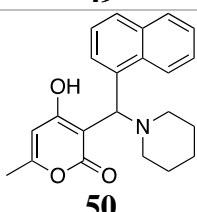
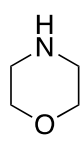
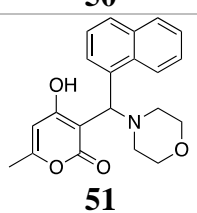
| ENTRY | AMINE | TIME (HRS) | PRODUCT | % YIELD |
|-------|---|------------|---|---------|
| 1 |  | 16 |  44 | 65 |
| 2 |  | 16 |  45 | 65 |
| 3 |  | 16 |  46 | 70 |

To extend the availability of Mannich bases, reaction in Scheme 15 was employed. The results for this reaction with selected amines are reported in Table 10. The same as with using *p*-nitrobenzaldehyde as the electrophile, 1-naphthaldehyde also shows reactivity towards Mannich reactions with different class of amines



Scheme 15: Mannich reaction of TAL, 1-naphthaldehyde, and amines

Table 10: Mannich reactions of TAL, 1-naphthaldehyde, and amines. Reaction conditions: TAL (0.5 mmol), naphthaldehyde (0.5 mmol), amine (0.5 mmol), AcOH_(cat.), and RT with stirring.

| ENTRY | AMINE | TIME (HRS) | PRODUCT | YIELD |
|-------|---|------------|---|-------|
| 1 |  | 16 |  47 | 31 |
| 2 |  | 24 |  48 | 25 |
| 3 |  | 24 |  49 | ✓ |
| 4 |  | 16 |  50 | 43 |
| 5 |  | 16 |  51 | 60 |

To support the proposed idea that AcOH is an efficient catalyst for the Mannich reaction, the effect of pH was taken into consideration as reported in Tables 11 and 12. The substrates selected were piperidine and morpholine due to the ease of isolation of the product, as well as obtaining both high yield and purity. The pH before the addition of cyclic amines and acid catalyst was between 6-7. The addition of amine followed by few AcOH (1 mol%) caused the pH to drop between 4-5. Few drops of H₂SO₄ caused the pH to drop to 2-3. After the completion of the reaction, the pH remains unchanged. It was determined that at slightly acidic pH, Mannich bases **44** and **46** were obtained in 51% and

52% yield, respectively, in 24 hours. In the absence of an acid catalyst, the reaction proceeds longer with lower yield with a slightly basic environment. While at very acidic condition, the products of interest were not obtained. This may be due to the protonation of amine that results in losing its ability to act as a nucleophile. These results support the claim that the reaction system is optimized when AcOH is used as the catalyst in Figure 7.

Table 11: pH dependence of Mannich reaction with piperidine. Reaction conditions: TAL (1.0 mmol), nitrobenzaldehyde (1.0 mmol), piperidine (1.0 mmol), DMM, and RT with stirring.

| Catalyst | Time (hrs) | Initial pH | pH after 1 hour | Final pH | % Yield of 21 |
|--------------------------------|------------|------------|-----------------|----------|---------------|
| H ₂ SO ₄ | 24 | 2-3 | 2-3 | 2-3 | 0 |
| AcOH | 16 | 4-5 | 5-6 | 5-6 | 51 |
| none | 24 | 6-7 | 7-8 | 7-8 | 30 |

Table 12: pH dependence of Mannich reaction with morpholine. Reaction conditions: TAL (1.0 mmol), nitrobenzaldehyde (1.0 mmol), morpholine (1.0 mmol), DMM, and RT with stirring.

| Catalyst | Time (hrs) | Initial pH | pH after 1 hour | Final pH | % Yield of 23 |
|--------------------------------|------------|------------|-----------------|----------|---------------|
| H ₂ SO ₄ | 24 | 2-3 | 2-3 | 2-3 | 0 |
| AcOH | 16 | 4-5 | 5-6 | 5-6 | 52 |
| none | 24 | 6-7 | 7-8 | 7-8 | 0 |

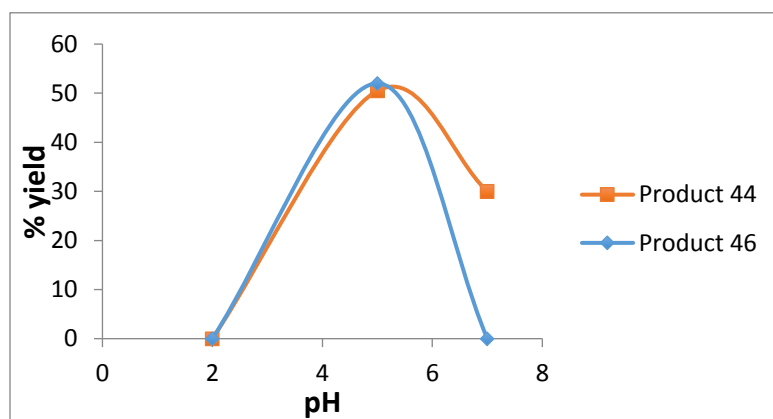


Figure 7: pH dependency of Mannich reaction at 24 hours reaction time

1.3 Conclusions

The efforts towards the development of bio-derived platform chemicals have been successful. The bio-based TAL molecule has prompted the interests of several researchers due to its high reactivity towards different transformations. Successful transformation of TAL to high-valued chemicals indicates TAL as potential biorenewable platform compound. Previously, our group has demonstrated several transformations of TAL, but not including its participation in Mannich reactions. The goal of this study is to develop efficient method that utilizes the bio-based TAL for the 3-component Mannich reaction. The success of this project results in the green synthesis of TAL-derived Mannich products.

This chapter has reported an efficient method to extend the library of 3-component TAL-derived Mannich bases. The current proposed method enhances cost efficiency by using only 1 mol% of the AcOH as catalyst in a single-pot reaction. The most noteworthy aspect of this approach is the utilization of the bio-based TAL as one of the starting materials. As a result of this work, the versatility of the bio-based TAL as a platform chemical has been further demonstrated *via* the 3-component Mannich reaction.

1.4 Experimental

All starting materials were purchased from Sigma-Aldrich and TCI America; solvents were purchased from Fisher Scientific and used without further purification. All reactions were carried out in flame-dried glassware flashed with argon in open air with stirring using a magnetic stir bar. All yields refer to isolated products by either column chromatography for liquid products, or washing with petroleum ether for solid products. Thin-layer chromatography (TLC) was performed using commercially available 250

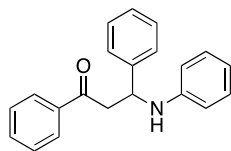
micron silica gel plates (Analtech) using UV light as a visualizing agent. Silica gel 60Å, particle size 0.032 – 0.063 mm, was used for flash column chromatography. ^1H and ^{13}C NMR spectra were acquired in CDCl_3 or DMSO-d on a Varian 400 MR or Bruker AVIII 600 MHz spectrometer. ^1H and ^{13}C chemical shifts (δ) are given in ppm relative to the residual protonated solvent peaks (CDCl_3 : $\delta_{\text{H}} = 7.26$ ppm, $\delta_{\text{C}} = 77.2$ ppm; DMSO-d : $\delta_{\text{H}} = 2.50$ ppm, $\delta_{\text{C}} = 39.5$ ppm) as an internal reference. Low-resolution mass spectra (LRMS) were recorded on an Agilent 6540 QTOF (quadrupole time of flight) mass spectrometer using ESI (electrospray ionization) or APCI (atmospheric-pressure chemical ionization) or EI (electron ionization) on an Agilent 6890 GC/MS.

Experimental, Physical, and Spectral Data

General Procedure: Typical Mannich reaction of TAL, aldehydes, and amines

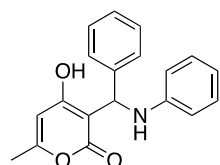
To a dried flask the commercially available 98% purity TAL (0.1261 g, 1.0 mmol) was added. Stoichiometric amount of aldehyde (1.0 mmol) was added, followed by the addition of DMM (5-6 mL). To this suspension, amine (1.0 mmol) was added and stirred. The resulting solution was added a catalytic amount of AcOH (1 mol%, 3 drops), then stirred at room temperature overnight. The resulting solid product was subjected to filtration. The filtrate was washed ten times with petroleum ether (1 mL x 10). The washed solid product was dried in air. For liquid product, crude was subjected to either preparative silica plates or silica column chromatography (silica gel, 67% EtOAc: 33% Hexane as an eluent) to obtain the product.

1,3-diphenyl-3-(phenylamino)propan-1-one (21)



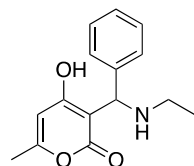
LRMS (ESI-QTOF) calcd for $C_{21}H_{19}NO$ [$M + H$]⁺ 302.1637, found 301.15.

4-hydroxy-6-methyl-3-(phenyl(phenylamino)methyl)-2H-pyran-2-one (22)



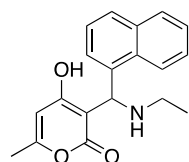
LRMS (ESI-QTOF) calcd for $C_{19}H_{17}NO_3$ [$M + H$]⁺ 308.1557, found 307.12.

3-((ethylamino)(phenyl)methyl)-4-hydroxy-6-methyl-2H-pyran-2-one (23)



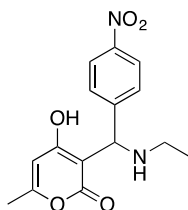
Yellow liquid. LRMS (ESI-QTOF) calcd for $C_{15}H_{17}NO_3$ [$M + H$]⁺ 260.1643, found 259.12.

3-((ethylamino)(naphthalen-1-yl)methyl)-4-hydroxy-6-methyl-2H-pyran-2-one (24)



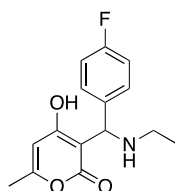
White solid (31.6% yield): ¹H NMR (400 MHz, DMSO-*d*) δ = 8.49 (d, 1H), 7.88-7.96 (m, 3H), 7.49-7.57 (m, 3H), 5.97 (s, 1H), 5.51 (s, 1H), 3.01 (q, 2H), 1.96 (s, 1H), 1.21 (t, 3H) ppm; LRMS (ESI-QTOF) calcd for $C_{19}H_{19}NO_3$ [$M + H$]⁺ 310.1692, found 309.14.

3-((ethylamino)(4-nitrophenyl)methyl)-4-hydroxy-6-methyl-2H-pyran-2-one (25)



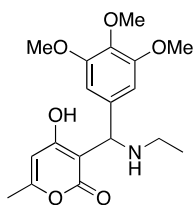
Pale yellow solid (88.4% yield): $^1\text{H NMR}$ (400 MHz, $\text{DMSO-}d$) δ = 8.21 (d, 2H), 7.78 (d, 2H), 5.48 (s, 1H), 5.27 (s, 1H), 2.87 (q, 2H), 1.96 (s, 1H), 1.16 (t, 3H) ppm; $^{13}\text{C NMR}$ (126 MHz, $\text{DMSO-}d$) δ = 178.1, 164.6, 159.5, 146.9, 146.4, 128.4, 123.5, 107.4, 90.3, 58.0, 40.7, 19.3, 11.2 ppm; LRMS (ESI-QTOF) calcd for $\text{C}_{15}\text{H}_{16}\text{N}_2\text{O}_5$ [$M + \text{H}$] $^+$ 305.1132, found 304.11.

3-((ethylamino)(4-fluorophenyl)methyl)-4-hydroxy-6-methyl-2H-pyran-2-one (26)



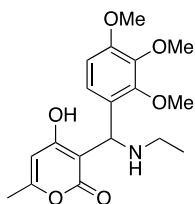
White solid (11.2%): $^1\text{H NMR}$ (400 MHz, $\text{DMSO-}d$) δ = 7.55 (t, 2H), 7.16 (t, 2H), 5.49 (s, 1H), 5.10 (s, 1H), 2.84 (t, 2H), 1.97 (s, 3H), 1.13 (t, 3H) ppm; LRMS (ESI-QTOF) calcd for $\text{C}_{15}\text{H}_{16}\text{FNO}_3$ [$M + \text{H}$] $^+$ 278.1416, found 377.11.

3-((ethylamino)(3,4,5-trimethoxyphenyl)methyl)-4-hydroxy-6-methyl-2H-pyran-2-one (27)



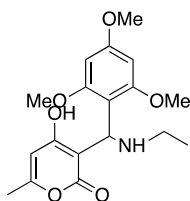
White solid (59.2% yield): $^1\text{H NMR}$ (400 MHz, $\text{DMSO-}d$) δ = 6.90 (s, 2H), 5.55 (s, 1H), 5.06 (s, 1H), 3.74 (s, 6H), 3.63 (s, 3H), 2.84 (q, 2H), 1.99 (s, 3H), 1.16 (t, 3H) ppm; LRMS (ESI-QTOF) calcd for $\text{C}_{18}\text{H}_{23}\text{NO}_6$ [$M + \text{H}$] $^+$ 350.1877, found 349.15.

3-((ethylamino)(2,3,4-trimethoxyphenyl)methyl)-4-hydroxy-6-methyl-2H-pyran-2-one (28)



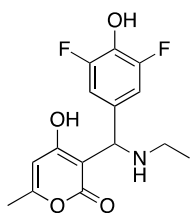
White solid (62.2% yield): $^1\text{H NMR}$ (400 MHz, $\text{DMSO-}d$) δ = 6.89 (s, 2H), 5.50 (s, 1H), 5.03 (s, 1H), 3.74 (s, 6H), 3.63 (s, 3H), 2.84 (q, 2H), 1.97 (s, 3H), 1.16 (t, 3H) ppm; $^{13}\text{C NMR}$ (126 MHz, $\text{DMSO-}d$) δ = 178.5, 164.2, 159.3, 152.9, 135.4, 135.1, 107.6, 105.2, 91.1, 60.2, 59.5, 59.3, 56.2, 56.1, 40.7, 19.5, 19.3, 11.4 LRMS (ESI-QTOF) calcd for $\text{C}_{18}\text{H}_{23}\text{NO}_6$ [$M + \text{H}$] $^+$ 350.1902, found 349.15.

3-((ethylamino)(2,4,6-trimethoxyphenyl)methyl)-4-hydroxy-6-methyl-2H-pyran-2-one (29)



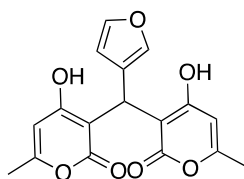
White solid (61.5%); $^1\text{H NMR}$ (400 MHz, $\text{DMSO-}d$) δ = 6.21 (s, 2H), 5.44 (s, 1H), 5.36 (s, 1H), 3.76 (s, 3H), 3.71 (s, 6H), 2.72 (d, 2H), 1.95 (s, 3H), 1.11 (t, 3H) ppm.

3-((3,5-difluoro-4-hydroxyphenyl)(ethylamino)methyl)-4-hydroxy-6-methyl-2H-pyran-2-one (30)



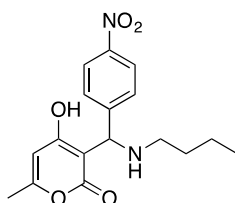
Pale pink solid (50.2% yield): $^1\text{H NMR}$ (400 MHz, $\text{DMSO-}d$) δ = 7.20 (q, 2H), 5.50 (s, 1H), 5.02 (s, 1H), 2.79-2.84 (m, 2H), 1.98 (s, 3H), 1.12-1.15 (m, 3H) ppm; LRMS (ESI-QTOF) calcd for $\text{C}_{15}\text{H}_{15}\text{F}_2\text{NO}_4$ [$M + \text{H}$] $^+$ 312.1318, found 311.10.

3,3'-(furan-3-ylmethylene)bis(4-hydroxy-6-methyl-2H-pyran-2-one) (31)



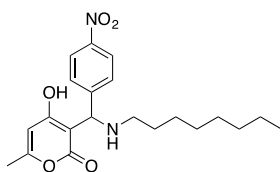
Yellow liquid; $^1\text{H NMR}$ (400 MHz, CHCl_3-d) $\delta = 7.20$ (s, 1H), 6.27 (q, 1H), 6.07 (d, 1H), 5.97 (s, 2H), 5.58 (s, 1H), 2.21 (s, 6H) ppm; LRMS (ESI-QTOF) calcd for $\text{C}_{17}\text{H}_{14}\text{O}_7$ [$M + \text{H}$] $^+$ 331.0807, found 330.07.

3-((butylamino)(4-nitrophenyl)methyl)-4-hydroxy-6-methyl-2H-pyran-2-one (32)



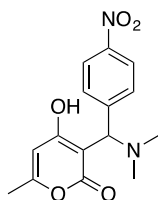
Pale yellow solid (75.2%); $^1\text{H NMR}$ (400 MHz, $\text{DMSO}-d$) $\delta = 8.21$ (d, 2H), 7.78 (d, 2H), 5.50 (s, 1H), 5.24 (s, 1H), 2.82-2.87 (m, 2H), 1.97 (s, 3H), 1.55 (q, 2H), 1.27-1.32 (m, 2H), 0.84 (t, 3H) ppm; LRMS (ESI-QTOF) calcd for $\text{C}_{17}\text{H}_{20}\text{N}_2\text{O}_5$ [$M + \text{H}$] $^+$ 333.1406, found 332.14.

4-hydroxy-6-methyl-3-((4-nitrophenyl)(octylamino)methyl)-2H-pyran-2-one (33)



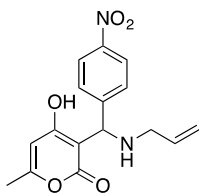
White solid (83.8%); $^1\text{H NMR}$ (400 MHz, $\text{DMSO}-d$) $\delta = 8.21$ (d, 2H), 7.78 (d, 2H), 5.49 (s, 1H), 5.24 (s, 1H), 2.81-2.86 (m, 2H), 1.97 (s, 3H), 1.55 (q, 2H), 1.27-1.32 (m, 10H), 0.84 (t, 3H) ppm; LRMS (ESI-QTOF) calcd for $\text{C}_{21}\text{H}_{28}\text{N}_2\text{O}_5$ [$M + \text{H}$] $^+$ 389.2028, found 388.20.

3-((dimethylamino)(4-nitrophenyl)methyl)-4-hydroxy-6-methyl-2H-pyran-2-one (34)



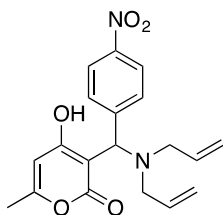
Bright yellow solid (17.0%); $^1\text{H NMR}$ (400 MHz, $\text{DMSO-}d$) δ = 8.22 (d, 2H), 7.83 (d, 2H), 5.52 (s, 1H), 5.25 (s, 1H), 2.65 (s, 6H), 1.97 (s, 3H) ppm; LRMS (ESI-QTOF) calcd for $\text{C}_{15}\text{H}_{16}\text{N}_2\text{O}_5$ $[M + \text{H}]^+$ 305.1095, found 304.11.

3-((allylamino)(4-nitrophenyl)methyl)-4-hydroxy-6-methyl-2H-pyran-2-one (35)



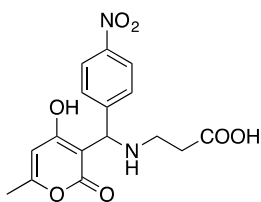
Pale yellow solid; $^1\text{H NMR}$ (400 MHz, CDCl_3 - d) δ = 8.19 (d, 2H), 7.67 (d, 2H), 5.88-5.90 (m, 1H), 5.83 (s, 1H), 5.32 (d, 1H), 5.28 (t, 1H), 5.10 (s, 1H), 3.34-3.50 (m, 2H), 2.18 (s, 3H) ppm; $^{13}\text{C NMR}$ (126 MHz, $\text{DMSO-}d$) δ = 177.7, 164.4, 159.6, 146.9, 146.3, 129.6, 123.6, 122.1, 107.0, 90.5, 57.8, 47.6, 19.3 ppm; LRMS (ESI-QTOF) calcd for $\text{C}_{15}\text{H}_{16}\text{N}_2\text{O}_5$ $[M + \text{H}]^+$ 317.1116, found 316.11.

3-((diallylamino)(4-nitrophenyl)methyl)-4-hydroxy-6-methyl-2H-pyran-2-one (36)



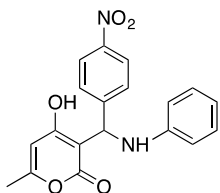
Yellow solid; $^1\text{H NMR}$ (400 MHz, CDCl_3 - d) δ = 8.34 (d, 1H), 8.13 (d, 1H), 8.03 (d, 1H), 7.70 (d, 1H), 5.80-5.88 (m, 2H), 5.73 (s, 1H), 5.24-5.30 (m, 4H), 5.04 (s, 1H), 3.46 (d, 3H), 3.38 (t, 1H), 1.96 (s, 3H); LRMS (ESI-QTOF) calcd for $\text{C}_{19}\text{H}_{20}\text{N}_2\text{O}_5$ $[M + \text{H}]^+$ 357.1452, found 356.14.

3-(((4-hydroxy-6-methyl-2-oxo-2H-pyran-3-yl)(4-nitrophenyl)methyl)amino)propanoic acid (37)



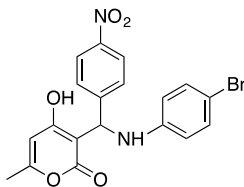
White solid; $^1\text{H NMR}$ (400 MHz, $\text{DMSO-}d$) δ = 8.40 (d, 2H), 8.07 (d, 2H), 5.90 (s, 1H), 5.50 (s, 1H), 2.32 (s, 1H), 2.24 (s, 3H), 2.21 (s, 1H), 2.13 (s, 2H) ppm; LRMS (ESI-QTOF) calcd for $\text{C}_{16}\text{H}_{16}\text{N}_2\text{O}_7$ [$M + \text{H}$] $^+$ 349.1039, found 348.10.

4-hydroxy-6-methyl-3-((4-nitrophenyl)(phenylamino)methyl)-2H-pyran-2-one (38)



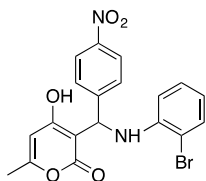
Yellow solid (54.3%); $^1\text{H NMR}$ (400 MHz, CHCl_3 - d) δ = 8.13 (d, 2H), 7.65 (d, 2H), 7.24 (d, 2H), 6.94 (t, 1H), 6.87 (d, 2H), 5.93 (s, 1H), 5.77 (s, 1H), 2.19 (s, 3H) ppm; $^{13}\text{C NMR}$ (126 MHz, $\text{DMSO-}d$) δ = 177.5, 164.3, 159.9, 146.9, 146.8, 133.3, 129.7, 128.9, 128.7, 128.6, 123.5, 106.7, 91.0, 58.7, 49.3, 19.3 ppm. LRMS (ESI-QTOF) calcd for $\text{C}_{19}\text{H}_{16}\text{N}_2\text{O}_5$ [$M + \text{H}$] $^+$ 353.1140, found 352.11.

3-(((4-bromophenyl)amino)(4-nitrophenyl)methyl)-4-hydroxy-6-methyl-2H-pyran-2-one (39)



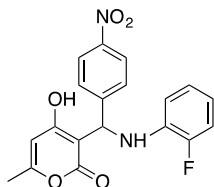
White solid; $^1\text{H NMR}$ (400 MHz, $\text{DMSO-}d$) δ = 8.06 (d, 2H), 7.58 (d, 2H), 7.24 (d, 2H), 6.66 (d, 2H), 5.92 (s, 1H), 5.74 (s, 1H), 2.14 (s, 3H) ppm.

3-(((2-bromophenyl)amino)(4-nitrophenyl)methyl)-4-hydroxy-6-methyl-2H-pyran-2-one (40)



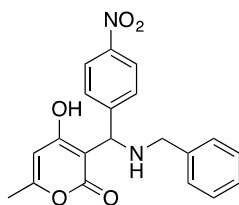
Yellow solid (62.0%); $^1\text{H NMR}$ (400 MHz, $\text{DMSO-}d$) δ = 8.19 (d, 2H), 7.69 (d, 2H), 7.50 (d, 1H), 7.18 (t, 1H), 6.74-6.82 (m, 2H), 6.00 (s, 1H), 5.88 (s, 1H), 2.20 (s, 3H) ppm; $^{13}\text{C NMR}$ (126 MHz, $\text{DMSO-}d$) δ = 168.7, 165.1, 163.0, 147.8, 143.0, 133.0, 129.0, 128.0, 124.2, 121.6, 114.4, 112.2, 101.7, 55.5, 20.0 ppm; LRMS (ESI-QTOF) calcd for $\text{C}_{19}\text{H}_{15}\text{BrN}_2\text{O}_5$ [$M + \text{H}$] $^+$ 431.0262, found 430.02.

3-(((2-fluorophenyl)amino)(4-nitrophenyl)methyl)-4-hydroxy-6-methyl-2H-pyran-2-one (41)



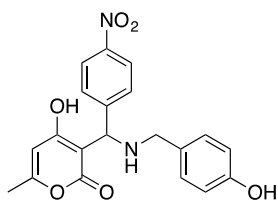
Yellow solid (37.2%); $^1\text{H NMR}$ (400 MHz, $\text{DMSO-}d$) δ = 8.17 (d, 2H), 7.65 (d, 2H), 7.06 (q, 1H), 6.91 (t, 1H), 6.72 (t, 1H), 6.61 (d, 1H), 6.10 (s, 1H), 6.01 (s, 1H), 2.16 (s, 3H) ppm; LRMS (ESI-QTOF) calcd for $\text{C}_{19}\text{H}_{15}\text{FN}_2\text{O}_5$ [$M + \text{H}$] $^+$ 371.1042, found 371.10.

3-((benzylamino)(4-nitrophenyl)methyl)-4-hydroxy-6-methyl-2H-pyran-2-one (42)



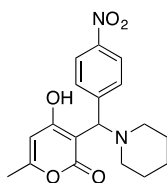
Pale yellow solid (75.3%); $^1\text{H NMR}$ (400 MHz, $\text{DMSO-}d$) δ = 8.19 (d, 2H), 7.71 (d, 2H), 7.35-7.40 (m, 5H), 5.59 (s, 1H), 5.20 (s, 1H), 4.01 (d, 2H), 2.01 (s, 3H) ppm; LRMS (ESI-QTOF) calcd for $\text{C}_{20}\text{H}_{18}\text{N}_2\text{O}_5$ [$M + \text{H}$] $^+$ 367.1586, found 366.12.

4-hydroxy-3-(((4-hydroxybenzyl)amino)(4-nitrophenyl)methyl)-6-methyl-2H-pyran-2-one (43)



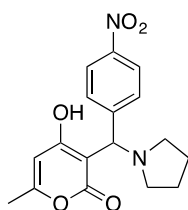
Dark yellow solid (72.3%); $^1\text{H NMR}$ (400 MHz, $\text{H}_2\text{O}-d$) δ = 8.21 (d, 2H), 7.66 (d, 2H), 7.30-7.34 (m, 4H), 5.73 (s, 1H), 5.35 (s, 1H), 4.09 (s, 2H), 1.95 (s, 3H) ppm; $^{13}\text{C NMR}$ (126 MHz, $\text{DMSO}-d$) δ = 177.8, 173.1, 166.3, 164.6, 159.3, 157.8, 131.2, 130.5, 128.4, 123.4, 115.3, 57.9, 49.03, 19.32 ppm; LRMS (ESI-QTOF) calcd for $\text{C}_{20}\text{H}_{18}\text{N}_2\text{O}_6$ [$M + \text{H}$] $^+$ 383.1244, found 383.12.

4-hydroxy-6-methyl-3-((4-nitrophenyl)(piperidin-1-yl)methyl)-2H-pyran-2-one (44)



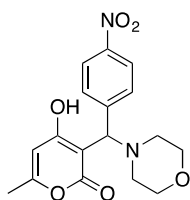
Pale yellow solid (64.6%); $^1\text{H NMR}$ (400 MHz, CHCl_3-d) δ = 8.13 (d, 2H), 7.67 (d, 2H), 5.71 (s, 1H), 4.89 (s, 1H), 3.57 (b, 1H), 2.79 (b, 1H), 2.54 (b, 1H), 2.09 (s, 3H), 1.79 (b, 7H) ppm; $^{13}\text{C NMR}$ (126 MHz, CHCl_3-d) δ = 175.4, 164.7, 162.0, 148.0, 144.4, 130.0, 124.3, 104.6, 97.5, 95.3, 70.0, 55.1, 24.8, 23.0, 20.0 ppm; LRMS (ESI-QTOF) calcd for $\text{C}_{18}\text{H}_{20}\text{N}_2\text{O}_5$ [$M + \text{H}$] $^+$ 344.1447, found 344.14.

4-hydroxy-6-methyl-3-((4-nitrophenyl)(pyrrolidin-1-yl)methyl)-2H-pyran-2-one (45)



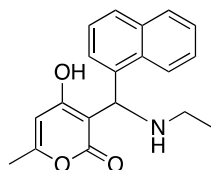
Bright yellow solid (65.0%); $^1\text{H NMR}$ (400 MHz, CHCl_3-d) δ = 8.13 (d, 2H), 7.68 (d, 2H), 5.71 (s, 1H), 4.91 (s, 1H), 3.59 (b, 1H), 2.80 (b, 1H), 2.56 (b, 1H), 2.09 (s, 3H), 1.75 (b, 5H) ppm; $^{13}\text{C NMR}$ (126 MHz, CHCl_3-d) δ = 175.6, 164.8, 162.0, 148.0, 144.4, 130.0, 124.3, 104.7, 95.2, 70.0, 24.8, 23.0, 20.0 ppm.

4-hydroxy-6-methyl-3-(morpholino(4-nitrophenyl)methyl)-2H-pyran-2-one (46)



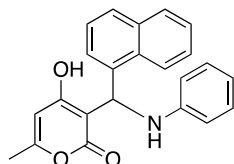
Bright yellow solid (70.0%); ^1H NMR (400 MHz, CHCl_3-d) δ = 8.14 (d, 2H), 7.58 (d, 2H), 5.80 (s, 1H), 4.67 (s, 1H), 3.74 (b, 5H), 3.11 (b, 1H), 2.50 (b, 2H), 2.14 (s, 3H) ppm; ^{13}C NMR (126 MHz, CHCl_3-d) δ = 169.4, 163.7, 163.0, 124.2, 101.5, 98.5, 90.3, 69.3, 66.5, 20.0 ppm; LRMS (ESI-QTOF) calcd for $\text{C}_{17}\text{H}_{18}\text{N}_2\text{O}_6$ [$M + \text{H}$] $^+$ 347.1243, found 346.12.

3-((ethylamino)(naphthalen-1-yl)methyl)-4-hydroxy-6-methyl-2H-pyran-2-one (47)



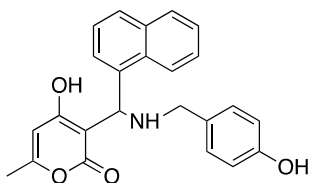
White solid (31.2%); ^1H NMR (400 MHz, $\text{DMSO}-d$) δ = 8.47 (d, 1H), 7.93 (d, 1H), 7.88-7.91 (m, 2H), 7.49-7.57 (m, 3H), 5.97 (s, 1H), 5.51 (s, 1H), 2.98 (q, 2H), 1.96 (s, 3H), 1.19 (t, 3H) ppm; LRMS (ESI-QTOF) calcd for $\text{C}_{19}\text{H}_{19}\text{NO}_3$ [$M + \text{H}$] $^+$ 310.1692, found 309.14.

4-hydroxy-6-methyl-3-(naphthalen-1-yl(phenylamino)methyl)-2H-pyran-2-one (48)



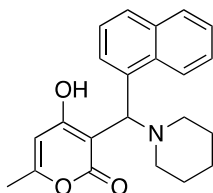
White solid (25.2%); ^1H NMR (400 MHz, $\text{DMSO}-d$) δ = 8.16 (q, 1H), 7.92 (q, 1H), 7.79 (d, 1H), 7.66 (d, 1H), 7.50 (q, 1H), 7.41 (t, 2H), 7.01 (t, 2H), 6.60 (d, 2H), 6.52 (t, 1H), 6.35 (s, 1H), 6.03 (s, 1H), 2.14 (s, 3H) ppm; ^{13}C NMR (126 MHz, $\text{DMSO}-d$) δ = 178.0, 166.7, 161.9, 147.7, 135.9, 133.51, 129.0, 128.8, 127.4, 126.1, 123.3, 121.2, 116.5, 1112.9, 101.1, 100.2, 48.9, 19.4 ppm; LRMS (ESI-QTOF) calcd for $\text{C}_{23}\text{H}_{19}\text{NO}_3$ [$M + \text{H}$] $^+$ 358.1728, found 357.14.

4-hydroxy-3-(((4-hydroxybenzyl)amino)(naphthalen-1-yl)methyl)-6-methyl-2H-pyran-2-one (49)



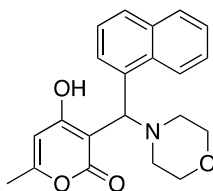
White solid; $^1\text{H NMR}$ (400 MHz, $\text{DMSO-}d$) δ = 7.93 (d, 2H), 7.88 (d, 1H), 7.79 (d, 1H), 7.48 (t, 2H), 7.43 (d, 1H), 7.22 (d, 2H), 6.80 (d, 2H), 5.89 (s, 1H), 5.63 (s, 1H), 4.03 (s, 2H), 2.03 (s, 3H) ppm; LRMS (ESI-QTOF) calcd for $\text{C}_{24}\text{H}_{21}\text{NO}_4$ [$M + \text{H}$] $^+$ 388.1538, found 387.15.

4-hydroxy-6-methyl-3-(naphthalen-1-yl(piperidin-1-yl)methyl)-2H-pyran-2-one (50)



White solid (43.4%); $^1\text{H NMR}$ (400 MHz, $\text{DMSO-}d$) δ = 8.54 (d, 1H), 8.01 (d, 2H), 7.94 (d, 1H), 7.89 (d, 1H), 7.50-7.60 (m, 3H), 5.99 (b, 1H), 5.60 (s, 1H), 3.32 (b, 2H), 2.88 (b, 1H), 1.98 (s, 3H), 1.49-1.70 (b, 7H) ppm; LRMS (ESI-QTOF) calcd for $\text{C}_{22}\text{H}_{23}\text{NO}_3$ [$M + \text{H}$] $^+$ 350.1711, found 349.17.

4-hydroxy-6-methyl-3-(morpholino(naphthalen-1-yl)methyl)-2H-pyran-2-one (51)



White solid (60.0%); $^1\text{H NMR}$ (400 MHz, $\text{DMSO-}d$) δ = 8.49 (d, 1H), 7.90 (q, 2H), 7.83 (d, 1H), 7.47 (m, 3H), 5.73 (s, 2H), 3.59-3.63 (m, 4H), 2.76-2.80 (m, 4H), 2.01 (s, 3H) ppm; LRMS (ESI-QTOF) calcd for $\text{C}_{21}\text{H}_{21}\text{NO}_4$ [$M + \text{H}$] $^+$ 352.1533, found 351.15.

1.5 References

- [1] Christian, D.G.; et al., *J. Sci Food Agric*, **2006**, 86, 1181-1188.
- [2] Vassilev, S.V.; et al., *Fuel*, **2010**, 89, 913–933.
- [3] Kiran, E.; et al., *J Chem Technol Biotechnol*, **2015**; 90, 1364–1379.
- [4] Bond, J.Q.; et al., *Science*, **2010**, 327, 1110–1114.
- [5a] Werpy, T.; Petersen, G., *Top Value Added Chemicals from Biomass Volume I – Results of Screening for Potential Candidates from Sugars and Synthesis Gas Top Value Added Chemicals From Biomass Volume I: Results of Screening for Potential Candidates*, **2004**.
- [5b] Wanninayake, U., Graduate Thesis and Dissertations, Iowa State University, 2016, paper xxxxx.
- [6] Bozell, J.; Petersen, G., *Green Chem.*, **2010**, 12, 539–554.
- [7] Koopman, F.; et al., *Bioresourc. Technol.*, **2010**, 101, 6291-6296.
- [8] Gandini, A.; et al., *J. Polym. Sci. Part A*, **2009**, 47, 295–298.
- [9] Eerhart, A.; et al., *Energy Environ. Sci.* **2012**, 5, 6407 – 6422.
- [10] Corma, A.; Iborra, S.; Velty, A., *Chem. Rev.* **2007**, 107, 2411.
- [11] Dijkman, W.P.; et al., *Angew. Chem. Int. Ed.*, **2014**, 53, 6515 –6518.
- [12] Jong, E.; et al., *Furandicarboxylic Acid (FDCA), A Versatile Building Block for a Very Interesting Class of Polyesters*, **2012**.
- [13] Whinfield, J.; et al., Br. Patent, 578079, filed July 29, 1941.
- [14] Hachihama, Y.; et al., *Technol. Rep. Osaka Univ.*, **1951**, 8, 475-480.
- [15] Moore, J.; Kelly, J., *Macromolecules*, **1978**, 11, 568-573.
- [16] Kato, S.; et al., A. Japanese patent application JP2008/291244, filed April 24, 2007.

- [17] Zhang, Z.; Deng, K., *ACS Catal.* **2015**, *5*, 6529–6544.
- [18] Qin, Y.; et al., *Green Chem.*, **2015**, *17*, 3718-3722.
- [19] Yi, G.; et al., *ChemSusChem*, **2014**, *7*, 2131 – 2137.
- [20] Zhou, C.; et al., *ChemCatChem*, **2015**, *7*, 2853 – 2863.
- [21] Gupta, N.K.; et al., *Green Chem.*, **2011**, *13*, 824-827.
- [22] Petrovska, B., *Pharmacogn Rev.*, **2012**, *6(11)*, 1–5.
- [24] Das, K.; et al., *W. J. Pharm. Pharm. Sci.*, **2016**, *5(2)*, 1099-1116.
- [25] Tran, V.L.; et al., *Tap Chi Hoa Hoc*, **2015**, *53(2)*, 243-246.
- [26] Burns, M., Graduate Thesis and Dissertations, University of York, 2010, paper 1059.
- [27] McGlacken, G.; Fairlamb, I., *Nat. Prod. Rep.*, **2005**, *22*, 369–385.
- [28] Chaturvedula, V.; et al., *J. Nat. Prod.*, **2002**, *65(7)*, 965–972.
- [29] Wang, Y.; et al., *Cancer Res.*, **2014**, *74(5)*, 1506-17.
- [30] Heimberger, J.; et al., *Biorg. Med. Chem. Let.*, **2015**, *25(6)*, 1192-1195.
- [31] Hatch, M.; et al., *Biochim. Biophys. Acta.*, **2002**, *1596*, 381-391.
- [32] Moreno-Manas, M.; Pleixats, R., *Naturally Occurring Oxygen Ring Systems*;
Academic: New York, 1992; p 21.
- [33] Moreno-Mañas, M.; Pleixats, R., *Adv. Hetero. Chem.*, **1992**, *53*, 1-84.
- [34] Chia, M.; et al., *J. Am. Chem. Soc.*, **2013**, *135*, 5699–5708.
- [35] Fairlamb, I.; et al., *Bioorg. Med. Chem.*, **2004**, *12*, 4285–4299.
- [36] Moody, C.; Rahimtoola, K., *J. Chem. Soc., Perkin Trans.* **1990**, *1*, 681.
- [37] Tang, S.; et al., *J. Am. Chem. Soc.* **2013**, *135*, 10099-10103.
- [38] Yalpani, M.; et al., *European J. Biochem.*, **1969**, *8*, 495-502.
- [39] Xie, D.; et al., *Biotech. and Bioeng.*, **2006**, *93(4)*, 726-736.
- [40] Cardenas, J.; Da Silva, N., *Metab. Eng.*, **2014**, *25*, 194–203.

- [41] Saunders, L.; et al., *J Ind Microbiol Biotechnol.*, **2015**, *42*, 711-721.
- [42] Collie, J., *J. Chem. Soc., trans.*, **1891**, *59*, 607-617.
- [43] Goel, A.; Ram, V., *Tetrahedron*, **2009**, *65*, 7865-7913.
- [44] Cheng, F.; Tan, S., *J. Chem. Soc.*, **1968**, *C*, 542-547.
- [45] Hansen, C.; Frost, J., *J. Am. Chem. Soc.*, **2002**, *124*, 5926-5927.
- [46] Loganayagi, C.; et al., *ACS Sust. Chem. Eng.*, **2014**, *2(4)*, 606-613.
- [47] de March, P.; et al., *J. Heterocyclic Chem.*, **1985**, *22*, 1537-1542.
- [48] Kraus, G.; et al., *Tetrahedron Letters*, **2016**, *57*, 1293–1295.
- [49] Kraus, G.; Wanninayake, U., *Tetrahedron Lett.* **2015**, *56*, 7112–7114.
- [50] Kraus, G.; et al., *Tetrahedron Letters*, **2015**, *56*, 3494–3496.
- [51] Burke, M.D., Schreiber, S.L., *Angew. Chem., Int. Ed.*, **2004**, *43*, 46.
- [52] Chen, W.; et al., *Org. Lett.*, **2010**, *12*, 3132.
- [53] Heravi, M.M.; et al., *Tetrahedron Lett.*, 2008, *49*, 6101.
- [54] Muller, F.L.; et al., *J. Am. Chem. Soc.*, **2005**, *127*, 17176.
- [55] Singh, M.S., Chowdhury, S., *RSC Advances*, **2012**, *2*, 4547–4592.
- [56] Nguyen, V., et al., *ACTA ABP Biochim. Polo.*, **2015**, *62(3)*, 547-552.
- [57] Muller, R., Goesmann, H., Waldmann, H., *Angew. Chem., Int. Ed.*, **1999**, *38*, 184.
- [58] Harvey, T.G., et al., *Corrosion Science*, **2011**, *53*, 2184–2190.
- [59] Namoussa, E.Y., Ouahrani, M.R., *Chemical Science Transactions*, **2015**, *4(4)*, 961-966.
- [60] Loto, R.T., et al., *J. Mater. Environ. Sci.*, **2012**, *3(5)*, 885-894.
- [61] Wang, M., et al., *Ind. J. of Chem.*, **2010**, *49(B)*, 1653-1656.
- [62] Wang, R., et al., *Tetrahedron Lett.*, **2007**, *48*, 2071–2073.

- [63] Iimura, S., et al., *Chem. Commun.*, **2003**, 1644–1645.
- [64] Li, Z., et al., *Journal of Molecular Catalysis A: Chemical*, **2007**, 272, 132–135.
- [65] Kidwai, M. et al., *Tetrahedron Lett.*, **2009**, 50, 1355–1358.
- [66] Kidwai, M., et al., *Catal. Commun.*, **2008**, 9, 2547–2549.
- [67] Phukan, P., et al., *Tetrahedron Lett.*, **2006**, 47, 5523–5525.
- [68] Kantam, M.L., et al., *Tetrahedron Lett.*, **2006**, 47, 5965–5967.
- [69] Onkara, P., et al., *Int. J. Pharm. Bio. Sci.*, **2013**, 4(2), 263 – 270.

CHAPTER II

CORROSION INHIBITION OF SMALL ORGANIC MOLECULES AND TRIACETIC ACID LACTONE MANNICH BASES

2.1 Introduction

2.1.1 Review of the electrochemistry of corrosion in mild steel (Fe)

Mild steel, also known as plain-carbon steel, is a material mainly composed of Fe that contains no more than 2% carbon. This type of steel is commonly used due to its low cost. Despite being inexpensive, mild steel has appreciable material properties such as ductility, malleability, and its ferromagnetic properties. As a result, it is widely used as a structural material in many industries such as automotive, ore, and petroleum.^[1]

However, mild steel has been known to have poor corrosion resistance when subjected to harsh reaction media.^[2] A common procedure for cleaning of industrial units made of mild steel is through acid treatment. The relatively high acidity makes industrial units prone to high level of corrosion. In order to preserve the material and its properties, surface coatings must be applied as corrosion inhibitors.

In order to further investigate the corrosion of Fe, it is worth mentioning the underlying concepts of the redox chemistry of Fe as it relates to corrosion process. Figure 1 shows the Pourbaix diagram of Fe in H₂O, which is constructed based on the Nernst equation in Equation 1.^[3a] This diagram provides information about the direction of an electrochemical process as a function of electrode potential in H₂O at varying pH.^[3b]

Although this diagram does not provide information about the kinetics of redox reaction, it contains information about the thermodynamically stable species of Fe at different conditions.^[4]

Furthermore, the diagram is helpful in predicting the three states of metal Fe namely: immunity, corrosion, and passivation. By definition, immunity is the state where metal Fe is thermodynamically stable, while corrosion is the active state of the metal. Passivation, on the other hand, is the event where Fe oxides or Fe salts form a protective layer in the metal surface that blocks active sites for corrosion. Moreover, the corrosion of Fe is initiated at two different regions in the Pourbaix diagram. The region at which the condition is highly reducing (low redox potential), $\text{H}_3\text{O}^+/\text{H}^+$ directs the formation of the stable Fe^{2+} species. At highly oxidizing conditions (high redox potential), the formation of the stable Fe^{3+} is promoted by O_2 . Using the Pourbaix diagram, the redox reaction equations for the formation of stable species are presented in Scheme 1.

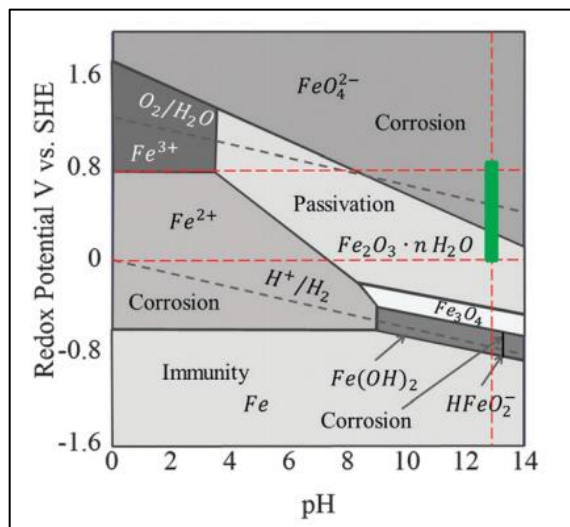
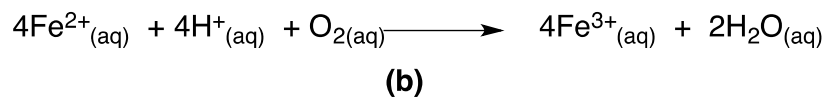
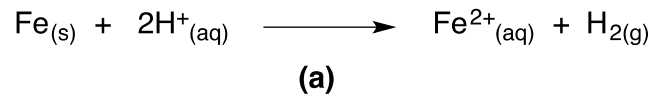


Figure 1: Pourbaix diagram of iron in water at 25°C as adapted from ref. 3a and 3b

$$E = E^{\circ} - \frac{0.059}{n} \log_{10} Q$$

Equation 1: Nernst equation at 25°C. E= cell potential at 25°C; E⁰= standard cell potential; n=moles of electrons transferred in the redox reaction; Q= reaction quotient.



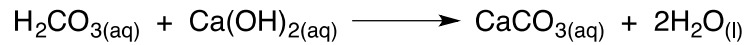
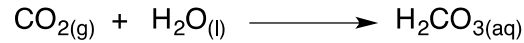
Scheme 1: Redox reactions for the formation of Fe²⁺ and Fe³⁺

2.1.2 Corrosion of reinforced steel in concrete and mild steel

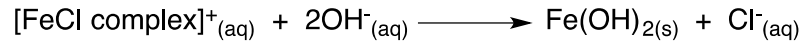
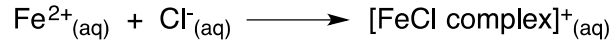
In the construction field, mixtures in reinforced concrete provide a tightly adhering film to the surface of the steel. The presence of this alkaline film acts as a protective layer that prevents steel from undergoing anodic reaction, a process known as passivation. Although this layer prevents corrosion due to direct contact with aqueous acids, there are other factors that induce corrosion such as Cl⁻, CO₂, H₂O, and O₂ as proposed by Raja and co-workers in Scheme 2.^[5] Moreover, Zhao and co-workers have studied corrosion expansion sensors in reinforced steel concrete and proposed a diagram for the system shown in Figure 2.^[6] While concrete provides a physical barrier against direct exposure of steel to corrosion agents, it consists of tiny pores where small gas molecules and small ions can permeate. This eventually results in the initiation of corrosion activity in the surface of the steel.

To discuss briefly, gaseous CO_2 permeates into the concrete in the presence of moisture to form H_2CO_3 . This then reacts with $\text{Ca}(\text{OH})_2$ from the concrete mixture to form CaCO_3 (calcite). Consequently, calcite drops the pH of the surrounding environment from 12-13 to less than 8, which promotes corrosion. In addition, O_2 gas molecules are also capable of permeating through the pores. This eventually leads to rusting of steel. Chloride ions present in the concrete mixture react with Fe^{+2} in the surface of the steel forming FeCl complexes.^[7] The alkalinity of the concrete provides OH^- , which reacts with FeCl complexes, liberating Cl^- and ferrous hydroxide. In the presence of H_2O and O_2 , ferrous hydroxide undergoes oxidation to ferric hydroxide, which is the hydrated species of rust.

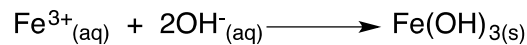
To suppress the rate of corrosion in steel, several widely manufactured inhibitors are used, such as calcium nitrate (CN), amine-alkanolamine derived inhibitors, and monofluorophosphate.^[8] In 2015, Raja and co-workers mentioned that there are two different classifications of corrosion inhibitors for reinforced steel in concrete.^[4] The first type is inorganic corrosion inhibitors that mostly contains nitrites. The second type is organic corrosion inhibitor, which contains alkanolamine and inorganic/organic salt mixtures. These inhibitors are known to form stable metal complexes that prevent the adsorption of aggressive corrosion agents to the metal surface. Although these anti-corrosion substrates provide excellent resistance for steel against corrosion, most of them are highly toxic to both human and the environment.



(a)



(b)



(c)

Scheme 2: Corrosion process in steel reinforcement in concrete.^[5] (a) Carbonic acid induced corrosion; (b) Chloride ion induced corrosion; (c) O₂ induced corrosion.

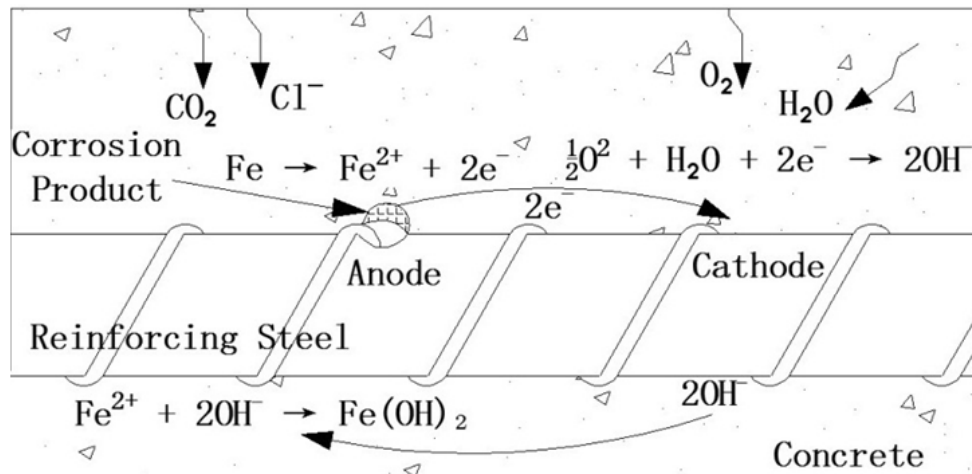
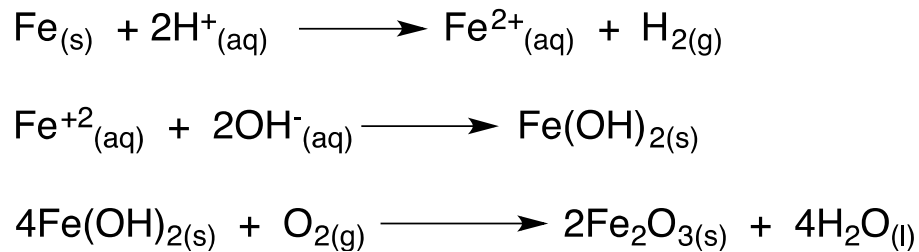


Figure 2: Diagram of Steel reinforcement in concrete as adapted from ref [6].

Unlike the different corrosion mechanisms possible for reinforced steel in concrete, the chemical reaction for the corrosion of mild steel in engineered structures is straightforward. As mentioned above, acid treatment for cleaning and other processes are the main cause of corrosion in mild steel in industry. This makes aqueous acid as the

leading initiator for the corrosion activity for mild steel in industrial settings. Moreover, molecular oxygen and moisture from the atmosphere also play minor roles in completing the rusting process as shown in Scheme 3. Briefly, mild steel and H^+ undergo a simultaneous redox reaction. The solid mild steel oxidizes to Fe^{2+} , while H^+ is reduced to gaseous H_2 . Furthermore, H_2O undergoes reduction under acidic condition to produce OH^- , which reacts with Fe^{2+} to form $Fe(OH)_2$.^[8] This eventually leads to oxidation of $Fe(OH)_2$ in the presence of atmospheric oxygen to Fe_2O_3 , which is the orange-red rust commonly observed in corroded steel.



Scheme 3: Acid-induced corrosion in mild steel

With the high demand of using mild steel as structural materials, the rate of corrosion should be controlled, if not completely suppressed. This can be done by the employment of three possible methods of surface protection: passive barrier protection, active protection, and sacrificial protection. The latter method includes coating of the steel surface with metallic, organic, and powdered materials. In this study, the use of organic molecules as corrosion inhibitors in mild steel will be evaluated.

2.1.3 Corrosion inhibition activity of organic molecules

Commercially manufactured inorganic corrosion inhibitors were evaluated to have negative impacts on human health and environment. Direct contact with these inhibitors were found to cause damage to organ systems.^[5] The hazards can be incurred during the synthesis of the compounds or during the coating process.^[9] Also, they can act as competitive inhibitors during normal enzymes-substrate interaction in biochemical processes.^[10] As a result, non-toxic organic molecules with corrosion inhibition activity are needed.

Some of the well-studied organic inhibitors for metals are molecules containing bonds with π -electrons and heteroatoms such as N, O, and S. Both π -electrons and lone pairs play specific roles to effectively decline the rate of corrosion of metals under wide array of environmental conditions.^{[11]-[13]} In addition, the presence of functional groups attached to the inhibitor's reactive center also affects the efficiency of organic inhibitors. For instance, a variety of substituted pyridines and anilines were screened for corrosion inhibition activity in steel. Tables 1 and 2 summarize some of the data reported by Donya and co-workers.^[14]

As presented in Table 1, the presence of C=C and halogens in aniline decreased the pK_a of the amine, which leads to a decrease in corrosion rate of metal, Similarly, when substituted pyridines were used as inhibitors, correlation between amine basicity and corrosion rate was also observed. By further evaluations, the authors concluded that inhibition activity of these compounds is governed by the protonated amine physically adsorbed at the metal surface.

Table 1: Corrosion inhibition activity of anilines^[14]

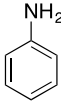
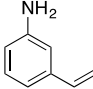
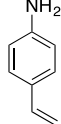
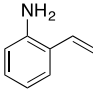
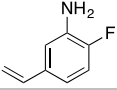
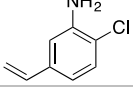
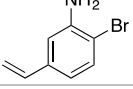
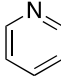
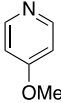
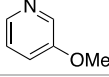
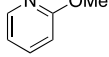
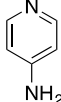
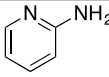
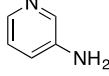
| ENTRY | AMINE | AMINE BASICITY, pK _a | CORROSION RATE (g/m ² h) |
|-------|--|------------------------------------|--|
| 1 |  | 4.58 | 1.793 |
| 2 |  | 4.36 | 1.589 |
| 3 |  | 4.15 | 1.557 |
| 4 |  | 3.97 | 1.571 |
| 5 |  | 2.72 | 1.428 |
| 6 |  | 2.39 | 1.311 |
| 7 |  | 2.29 | 1.304 |

Table 2: Corrosion inhibition activity of pyridines^[14]

| ENTRY | AMINE | AMINE BASICITY, pK _a | CORROSION RATE (g/m ² h) |
|-------|---|------------------------------------|--|
| 1 |  | 5.23 | 1.700 |
| 2 |  | 6.62 | 1.949 |
| 3 |  | 4.88 | 1.643 |
| 4 |  | 3.28 | 1.404 |
| 5 |  | 9.17 | 2.504 |
| 6 |  | 6.86 | 1.996 |
| 7 |  | 5.98 | 1.830 |

In 2011, Harvey and co-workers evaluated the anti-corrosion activity of other substituted aromatics and heterocyclic compounds.^[15] The corrosion inhibition test was employed on two aluminium alloys named AA2024 and AA7075. The former contained the following alloying components: 5.3% Cu, 1.6% Mg, 0.6% Mn, 0.2% Fe, and <0.1% Zn. The latter composed of the following metals: 1.4% Cu, 2.4% Mg, <0.1% Mn, 0.2 % Fe, and 5.4% Zn. Table 3 summarizes selected inhibitors with anti-corrosion activities, while Table 4 contains compounds that accelerated both the corrosion of AA2024 and AA7075.

From this work, several conclusions were made about the effects of different atoms, functional groups, and substituent position in the aromatic ring to the corrosion activity. The strength of coordination of these compounds with the alloying metal was also briefly discussed. For instance, it was mentioned the replacement of C atom with N in aromatic compounds shows a negative effect to the corrosion inhibition activity in AA2024 in Table 3, Entries 3 and 4. The activity was reversed for AA7075, on the other hand, such that the N-substituted aromatic has shown better anti-corrosion activity in Entries 8 and 12 in Table 3. The authors claimed that this opposing effect is due to the coordination of N lone pairs and metal impurities present in aluminium alloy.^[15] In AA7075, there is a higher Zn content compared to AA2024. The stronger interaction of N lone pair with Zn creates a chelating effect. The metal complex, as a consequence, forms a protective layer at the surface of the metal that inhibits corrosion. On the other case, the strong S-Cu interaction governs the corrosion inhibition activity in AA2024.^[15]

Furthermore, it was also discussed that both carboxylate (-COOH) and hydroxyl (-OH) groups shows minimal improvements to the corrosion inhibition activity. However,

this occurrence is only observed when the parent compound is a corrosion promoter.^[15] Substituents in the ortho and para positions of aromatic compounds, relative to the most inhibiting group, enhance the anti-corrosion activity. The positive inhibition activity of ortho and para substituted aromatics is due to the enhancement of electron density of the inhibiting groups at these position. As observed in the literature, not all compounds bearing lone pairs and π electrons act as corrosion inhibitors as shown in Table 4.^{[14],[15]} If the chelation of metals and chelating agent is too strong, it will result into the dissolution of metal surface forming soluble complexes.^[16] As soluble complexes leave the metal surface, it exposes the active site for corrosion promoters to attack. This results in the increases of the rate of metal corrosion.

Table 3: Anti-corrosion efficiency for metal sample AA2024 and AA7075^[15]

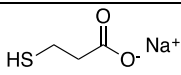
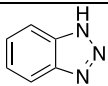
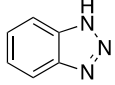
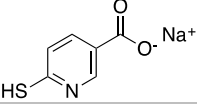
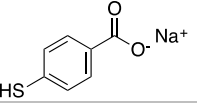
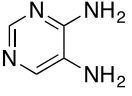
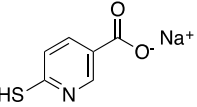
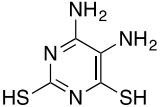
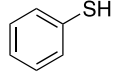
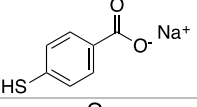
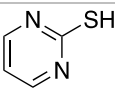
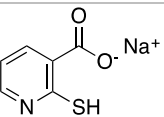
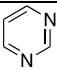
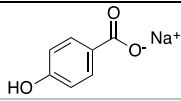
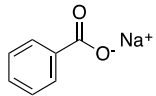
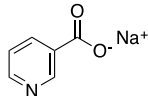
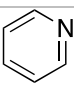
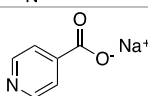
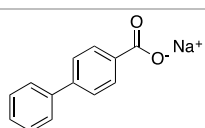
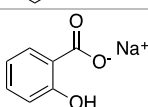
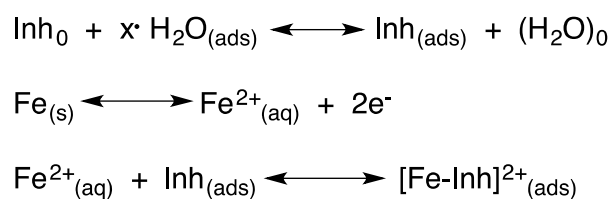
| ENTRY | INHIBITOR | INHIBITION EFFICIENCY (%) (AA2024) | ENTRY | INHIBITOR | INHIBITION EFFICIENCY (%) (AA7075) |
|-------|---|------------------------------------|-------|---|------------------------------------|
| 1 |  | 100 | 7 |  | 92 |
| 2 |  | 98 | 8 |  | 86 |
| 3 |  | 97 | 9 |  | 84 |
| 4 |  | 94 | 10 |  | 80 |
| 5 |  | 93 | 11 |  | 76 |
| 6 |  | 89 | 12 |  | 70 |

Table 4: Corrosion accelerators for both metal sample AA2024 and AA7075^[15]

| ENTRY | COMPOUND | ENTRY | COMPOUND |
|-------|---|-------|---|
| 1 |  | 5 |  |
| 2 |  | 6 |  |
| 3 |  | 7 |  |
| 4 |  | 8 |  |

In 1964, Bockris and co-workers established that the interaction between organic molecules and metals is a surface phenomena.^[17] The replacement of water from the metal surface by the inhibitor is a downhill process, thus, initiates the inhibition.^[18] For the corrosion inhibition of organic molecules in mild steel, a series of chemical reactions is proposed, as shown in Scheme 4. It is important to note that the series of reactions in Scheme 4 was proposed based on the original study on n-decylamine adsorption on solid metal electrode.^[17] For this system, the only factor affecting organic molecule-metal interaction is the covalent interaction between the lone pair of nitrogen and the empty d-orbital of the metal. This process is also known as chemical adsorption or chemisorption.



Scheme 4: Surface inhibition of organic molecules in Fe. Inh= inhibitor; x= number of molecules; 0 denotes free species in solution; ads denotes adsorbed in the metal surface.

Furthermore, not only chemisorption governs corrosion inhibition of organic compounds, but also physical adsorption (or physisorption). Several studies have recognized two possible modes of physisorption namely: physisorption of charged-inhibitors and physisorption of π -electrons.^{[18]-[20]} In acidic conditions, lone pair bearing atoms such as S, N, and O exist as protonated species forming positively charged moieties.^[21] The surface of the metal contains anions of the electrolyte creating a partially-negative field. This results in electrostatic interaction between the protonated atom of the inhibitor and the induced negative charge on the metal surface. The second mode of physisorption, is governed by the metal- π non-covalent interaction between electron-rich alkene, alkyne, or aromatics and the electron-deficient metal. Although the adsorption mechanism of corrosion inhibition varies for different organic compounds, both covalent and non-covalent interactions block the active site for corrosion agents to bind. These modes of adsorption suppress the corrosion activity.

2.1.4 Biobased TAL derivatives and Mannich bases as corrosion inhibitors in mild steel

There are many other known organic corrosion inhibitors in mild steel, presently. For example organophosphonic acid, aromatics, hydrazones, and thiourea derivatives were all studied to be effective as corrosion inhibitors in acidic media.^{[14],[15],[22]-[24]} Not only synthetic organic compounds show anti-corrosion activity, but natural products such as the leave extracts of pineapple, *Pulicaria crispa* (which belongs to the sunflower family), and *Osmanthus fragran* were also reported to cause a drastic improvement to mild steel's resistance against corrosion in acidic environment.^{[21],[25],[26]} The anti-corrosion activity of these natural products, moreover, were claimed to be due to the phenolic constituents of

the extracts capable of interacting with the surface of the metal. Figure 3a shows the phenolic components of ethanolic extracts of pineapple as reported by Ma and co-workers.^[27] The authors concluded that the characteristic trend of the direct relationship between the inhibition efficiency and temperature suggests a chemisorption mechanism. In other words, the hydroxyl groups in each component in the pineapple leaf extracts played the major active moiety that provides anti-corrosion activity.

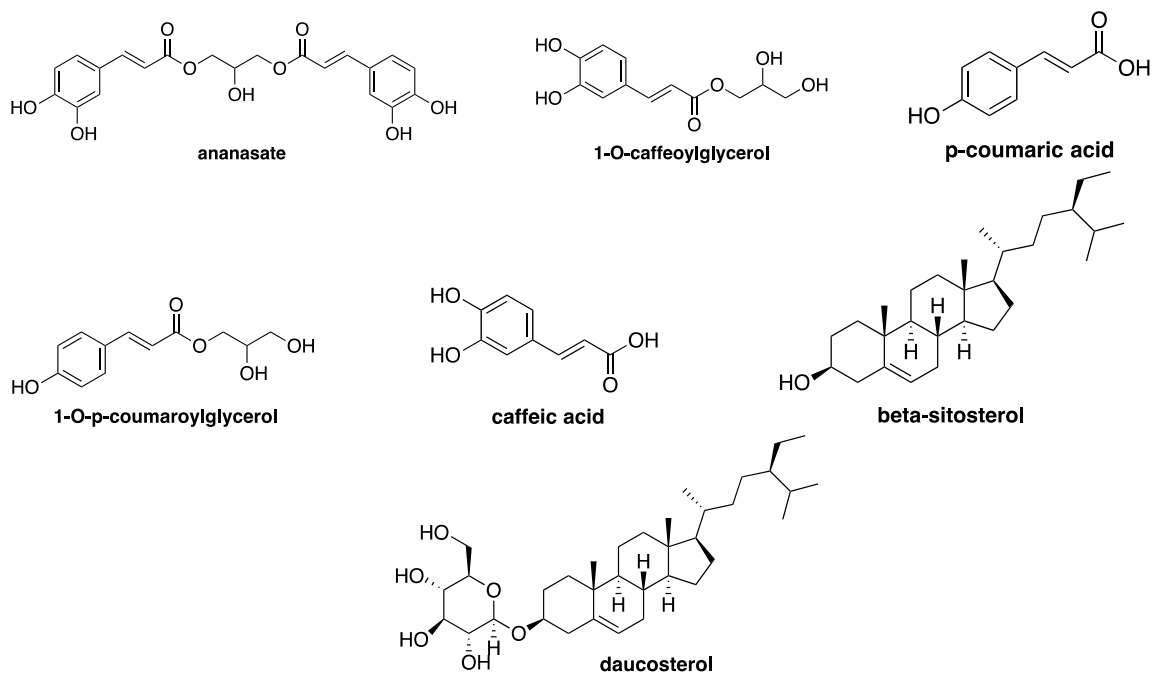


Figure 3a: Phenolic components in ethanolic extract of pineapple leaves^[27]

As demonstrated in the corrosion inhibition studies of leaf extracts, bulky and well-functionalized molecules from natural products are capable of inhibiting corrosion in mild steel. However, not only big molecules have anti-corrosion activity, but also small molecules such as the TAL derivative, *opuntiol 13* in Figure 3b.^[28] This compound is the major component in *Opuntia elatior* together with proline, campesterol, betacyanin, and

linolenic acid. Opuntiol can be synthesized from TAL in three-steps as reported elsewhere.^{[29],[30]} First is the O-methylation of TAL with K_2CO_3 and Me_2SO_4 , then, oxidation of position 7 to aldehyde using SeO_2 followed by reduction to alcohol. Studies show high anti-corrosion activity when using **13** as a corrosion inhibitor in mild steel under H_2SO_4 and HCl media. Furthermore, Mannich bases containing the TAL moiety were also showed activity against corrosion in Fe metal under H_3PO_4 .^[31] Both compounds **52** and **53** have shown anti-corrosive effects, with compound **53** showing a slightly better inhibition activity than **52**. The authors claimed that the methoxy group may have increased the polarizability and surface interaction of the inhibitor and the metal.^[31] This results into a better protective layer formed by **53**, decreasing the access to the Fe active site for corrosion.

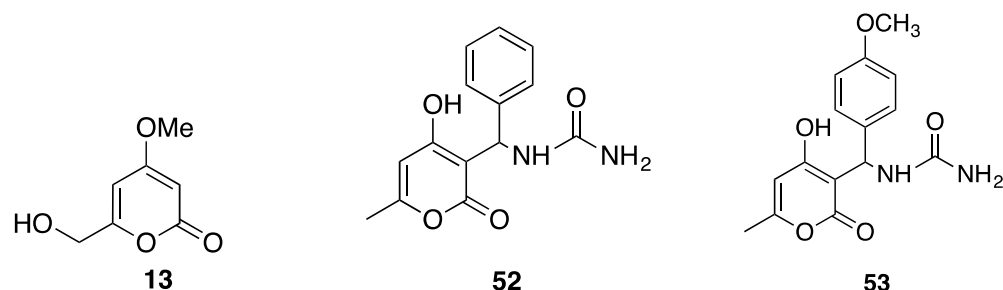


Figure 3b: TAL-based molecules with anti-corrosion activity.

In Chapter 1, the versatility of the TAL as platform chemical was discussed. One-pot synthesis of TAL-based Mannich bases was also achieved. In this current chapter, the corrosion inhibition activity of TAL derivatives, pyridines, and TAL-based Mannich bases will be evaluated. The evaluation of the anti-corrosion activity of these molecules is based on the previously studied, *opuntiol*. Comparison of the inhibition efficiency of these

organic molecules with the industrially-used corrosion inhibitors is not included in this current study and will be investigated separately.

2.2 Results and Discussions

In efforts to explore the applications of TAL derivatives, pyridines, and TAL-based Mannich bases, we have extended our studies to testing these compounds for corrosion inhibition activity in mild steel. Anti-corrosion activity of 2-pyrones, substituted pyridines, and Mannich bases were screened by Potentiostatic Electrochemical Impedance Spectroscopy (PEIS). In the current study, 0.1 M Na₂SO₄ was used as the electrolyte and inhibitor concentration of 1.0 mM. The pH was adjusted between 2.70 and 2.80 by the addition of H₂SO₄ to promote a corrosive environment. PEIS analysis produces data in a form of Nyquist plot, which is a characteristic semi-circle graph. The generation of Nyquist plot is based on equivalent circuit shown in Figure 4a. This model assumes the impedance curve does not create a negative loop. For impedance curves consisting of a loop, the circuit can be represented as in Figure 4b. It has been reported in the literature that the simplified circuit in Figure 4a provides a good first approximation calculation for the inhibition efficiency. Therefore, it was also used as a model circuit in this study.

The Nyquist plot provides information about the resistance of the electrolyte solution and the resistance experienced by the electron as it travels from the metal into the solution. The charge separation (capacitance) created between the solution and the metal surface can also be determined. The % IE of each inhibitor was calculated using Equation 2, where the R_{CT} was calculated using the relation in Equation 3. The uncertainty reported

is based only on actual experimental errors and does not include the uncertainty of the instrument.

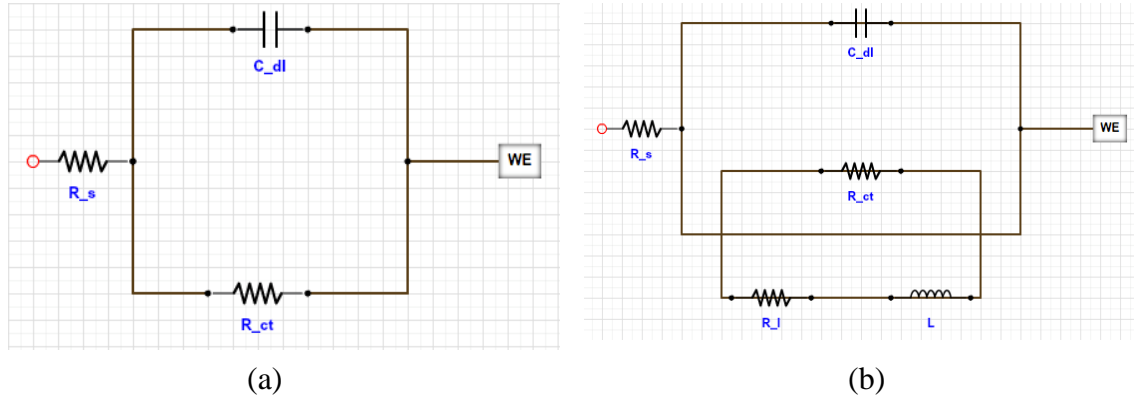


Figure 4: Equivalent circuit diagram. R_s = electrolyte resistance; R_{CT} = charge transfer resistance; C_{dl} = double layer capacitor; R_l = inductive resistance; L = inductive loop; WE= working electrode.

$$\%IE = \frac{R_{CT} - R_{CT0}}{R_{CT}} * 100\%$$

Equation 2: % Inhibition efficiency. R_{CT} = charge transfer resistance with the inhibitor; R_{CT0} = charge transfer resistance without the inhibitor

$$\text{Charge transfer resistance} = (x_2, 0) - (x_1, 0)$$

Equation 2: Charge transfer resistance as calculated from the Nyquist plot. $(x_2,0)$ and $(x_1,0)$ are the final and initial y-intercepts of the curve, respectively.

Knowing the high anti-corrosion activity of **13** reported from the literature, it was used as the control.^[28] Previous corrosion inhibition testing was employed to 2-pyrones including DAA, **13**, and **54**, at 60, 80, 100 ppm, respectively, in $H_2SO_{4(aq)}$ medium. It was found that **13** shows the best anti-corrosion activity followed by **54** with %IE of 28.8% and 23.6%, respectively. DHA did not show appreciable activity with %IE of -4.7% in $H_2SO_{4(aq)}$ electrolyte. Loganayagi and co-workers claimed that the corrosion inhibition of **13** is due to physisorption mechanism.^[28] Compounds **13** and **54** can be oriented in-plane

with the metal surface that enhances the metal- π electrons interaction. For DHA, the methyl and acetyl substituents in the 2-pyrone unit may have caused bond strains. This may lead to forbidding the lactone ring to be oriented in-plane for non-covalent interaction with the metal.

To further demonstrate the ability of 2-pyrones to suppress corrosion, the electrolyte from the previous test was replaced with 0.1 M $\text{Na}_2\text{SO}_{4(\text{aq})}$. The inhibitors were employed at a concentration of 1.0 mM (1.40×10^4 ppm). Based on the impedance analysis in Figure 5, DHA exhibited 25.6 %IE, while **54** provided 26.7% in Table 5. Other 2-pyrones were also evaluated for anti-corrosion activity as presented in Table 5. With all the tested 2-pyrones, **54** and DHA show the best %IE and **55** and TAL has the least anti-corrosion activity as shown in Scheme 5.

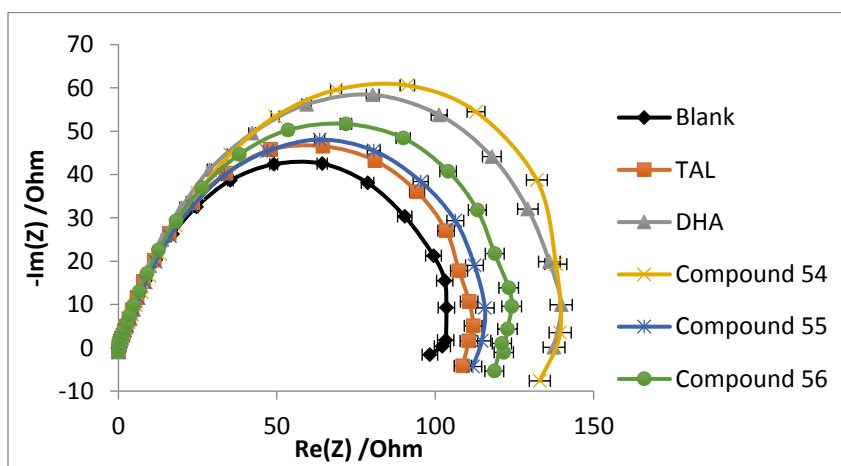
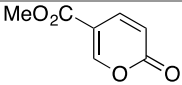
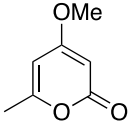
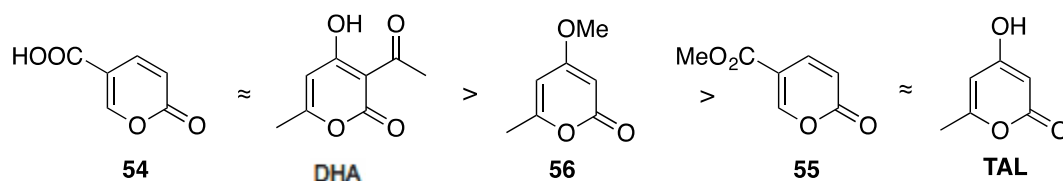


Figure 5: Nyquist plot of 2-pyrone compounds

Table 5: Corrosion inhibition activity of 2-pyrones

| Entry | Compound | R_{CT} (Ohms) | %IE \pm 2.5% |
|-------|--|-----------------|----------------|
| 1 | blank | 102.25 | 0 |
| 2 | TAL | 110.62 | 7.6 |
| 3 | DHA | 137.51 | 25.6 |
| 4 | <chem>CC(=O)C1=CC=C(O)O1</chem> 54 | 139.43 | 26.7 |

| | | | |
|----------|--|--------|------|
| 5 |  55 | 111.87 | 8.6 |
| 6 |  56 | 121.03 | 15.5 |



Scheme 5: Corrosion inhibition activity trend for 2-pyrones

It has been established that N is an effective atom for metal-lone pair interaction.^[11]

^[13] Several substituted pyridines were tested for corrosion inhibition activity in Table 6. Based on the Nyquist plot in Figure 6, **57** and **58** show the best inhibition. The decrease in %IE when the carbonyl group of the pyridine is in the *-ortho* position (**57** and **58**) versus the *-meta* position (**59** and **60**), in Scheme 6, can be due to the diminished electron density in the *-meta* position of an aromatic ring. This effect was also observed in a study elsewhere.^[15] To the best of our knowledge, the anti-corrosion activity of compounds **58** and **60** has never been reported in the literature.

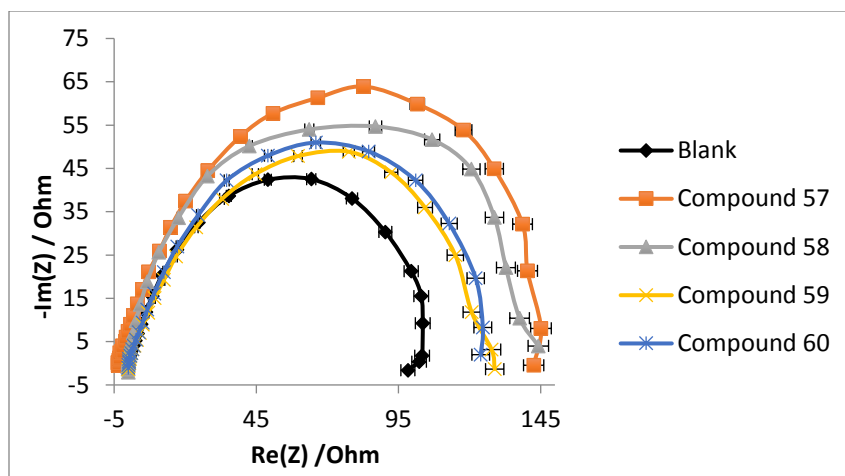
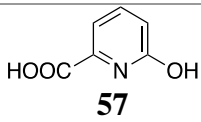
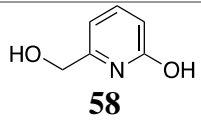
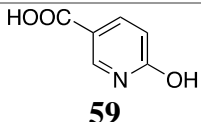
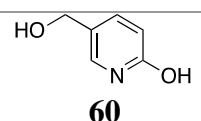
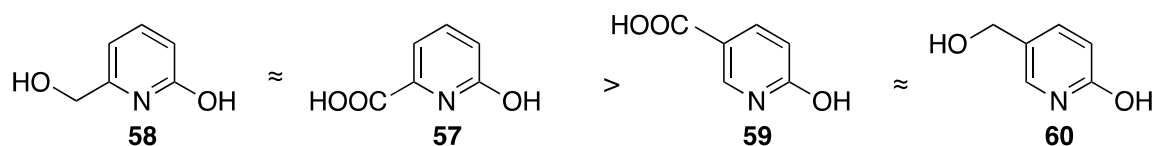


Figure 6: Nyquist plot of substituted pyridines

Table 6: Corrosion inhibition activity of substituted pyridine

| Entry | Compound | R_{CT} (Ohms) | %IE \pm 2.5% |
|-------|--|-----------------|----------------|
| 1 | blank | 102.25 | 0 |
| 2 |  57 | 142.52 | 30.0 |
| 3 |  58 | 146.27 | 29.5 |
| 4 |  59 | 128.83 | 20.7 |
| 5 |  60 | 123.92 | 17.5 |



Scheme 6: Corrosion inhibition activity trend for substituted pyridines

Using **58** as the reference compound, the effect of the replacement of C atom by N in an aromatic ring was also studied in Table 7. As presented in Entry 1 Table 7, **61** attained %IE of 17.8%, while **58** has shown %IE of 29.5% in Entry 3, Table 6. Compound **62** has shown better anti-corrosion activity when two carbon atoms were replaced by nitrogen atoms compound **63**. The trend in Scheme 7 can be attributed to the strong electron donor-acceptor interaction between N lone pair and the empty d-orbital of the metal. This observation was also reported elsewhere.^[15] To the best of our knowledge, the anti-corrosion activity of compound **63** has never been reported in the literature.

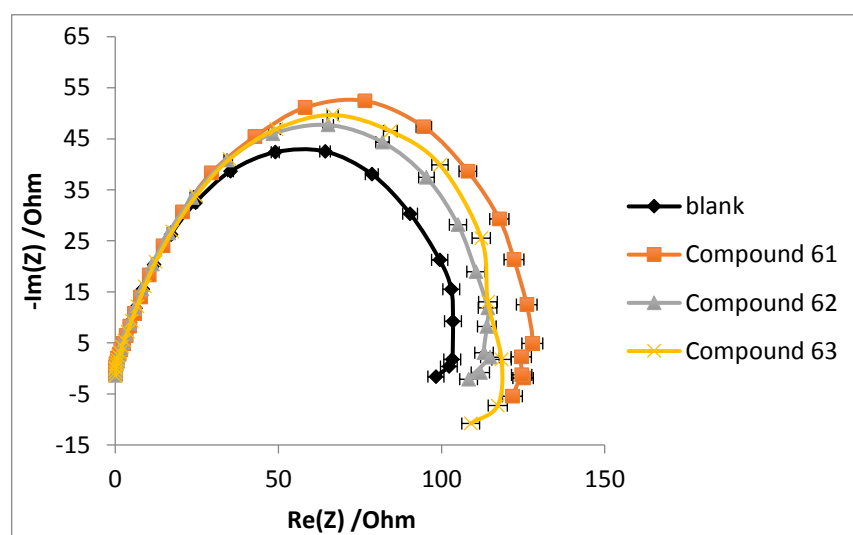
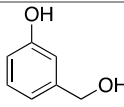
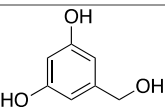
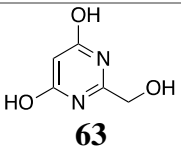
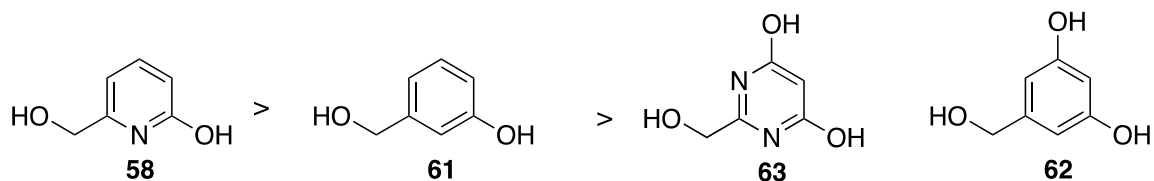


Figure 7: Nyquist plot of some aromatics

Table 7: Corrosion inhibition activity of some aromatics

| Entry | Compound | R _{ct} (Ohms) | %IE ± 2.5% |
|-------|--|------------------------|------------|
| 1 | blank | 102.25 | 0 |
| |  61 | 124.44 | 17.8 |
| 2 |  62 | 114.86 | 11.0 |

| | | | |
|---|--|--------|------|
| 3 |  <p style="text-align: center;">63</p> | 118.41 | 13.7 |
|---|--|--------|------|



Scheme 7: Corrosion inhibition activity trend of some aromatics

Mannich bases synthesized in Chapter 1 of this study were also evaluated for corrosion inhibition activity. Table 8 shows the corrosion inhibition activity of Mannich bases containing cyclic amine. All Mannich bases **44**, **46**, and **50** were found to promote corrosion as shown in Figure 8. Previous literatures published that in cases where the metal complex formed is soluble, then dissolution from the metal surface into the solution occurs.^[15] This leaves the bulk Fe surface exposed to corrosion agents. As a result, it was thought that the Fe complex of Mannich bases **44**, **46**, and **50** are soluble.

Furthermore, Jeeva and co-workers conducted corrosion inhibition studies with urea-derived Mannich bases.^[19] The anti-corrosion effect of changing one component from piperidino and pyrrolidino to morpholino ring were investigated. They have reported an enhanced anti-corrosion activity from morpholino to piperidino due to O atom's additional non-covalent interaction with the bulk Fe surface. The higher charge transfer resistance of **44** than **46**, in Figure 8, can be incurred to the mechanism proposed by Jeeva and co-workers. It is important to note that in the pH condition employed in this study, N can be in its protonated form. Also, SO_4^{2-} in the solution tends to adsorb to the metal-solution interface creating a local negatively-charged surface. This results into electrostatic

attraction between two oppositely charged species. The significant drop of the charge transfer resistance between **44** and **50** may be attributed to the lesser accessibility of the N lone pair. Compound **50** contains the more bulky naphthalene that may hinder donor-acceptor interaction between N lone pair and the metal's d-orbital.

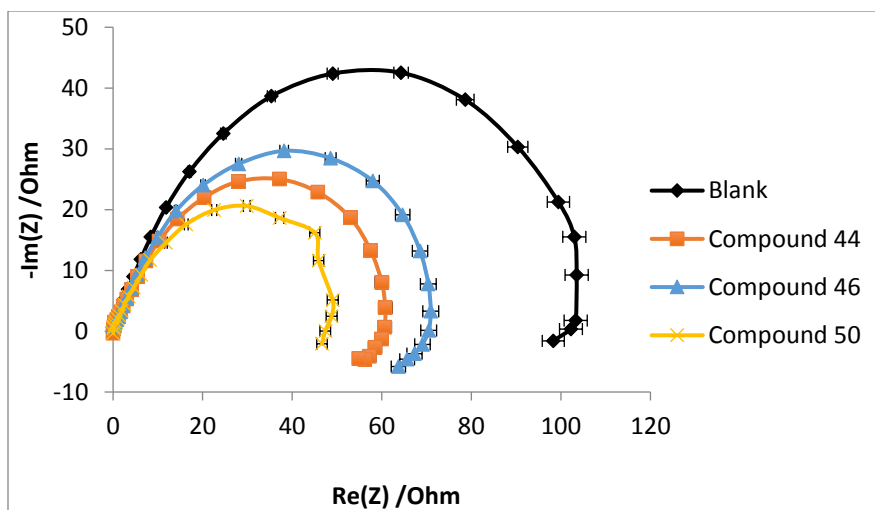
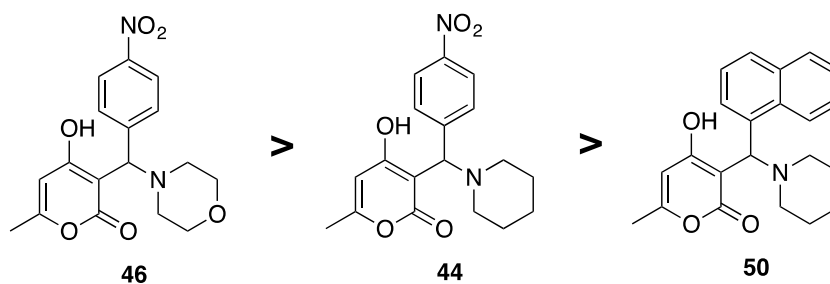


Figure 8: Nyquist plot of Mannich bases containing cyclic amine

Table 8: Corrosion inhibition activity of Mannich bases containing cyclic amine

| Entry | Compound | R_{CT} (Ohms) | %IE \pm 2.5% |
|-------|-----------|-----------------|----------------|
| 1 | blank | *102.25 | 0 |
| 2 | 44 | 60.66 | -69.9 |
| 3 | 46 | 70.94 | -45.3 |
| 4 | 50 | 46.66 | -120.9 |



Scheme 8: Corrosion inhibition activity trend of Mannich bases containing cyclic amine

Other Mannich bases containing aliphatic and aromatic amines were also evaluated in Table 9. Other than the corrosion activity of **25**, compounds **32**, **34**, **41**, and **42** acted as corrosion promoters rather than inhibitors as shown in Figure 9. Comparing the inhibition activities of Mannich bases in Table 8 and compound **25**, it was suspected that access to the lone pair of electrons in N plays a crucial role. Thus, it was hypothesized that the less hindered the amino moiety of the TAL-derived Mannich bases, the better %IE.

In Scheme 9 shows the trend of anti-corrosion activity of the Mannich bases tested. The depression of %IE from **25** and **32** to **34** supports the hypothesis claimed such that ethylamino is the least hindered and the dimethylamino group is the most hindered. Out of all Mannich bases tested in Table 9, only **25** has shown a positive efficiency value, while the rest have shown negative efficiency. The geometry of compounds **25** and **34** were optimized to visualize the orientation of the molecules shown in Figure 10. Compounds **41** and **42** are more hindered than **32**, the former exhibits better %IE than the latter. This can be attributed to the presence of the aromatic ring in **41** and **42**. In **41** and **42**, the benzyl substituent may have reoriented the molecule so that the electron-rich benzyl interacts with the electron-poor nitrobenzene *via* π -stacking. This reorientation exposed the lone pair of electrons of N to interact with the metal surface, thus, the better charge transfer resistance.

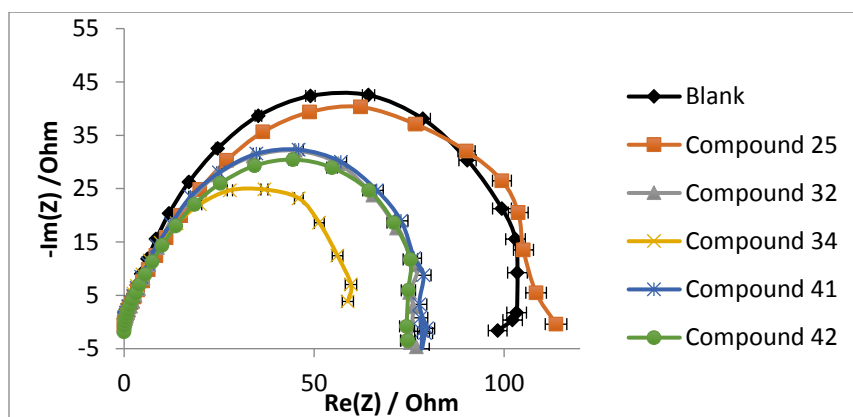


Figure 9: Nyquist plot of Mannich bases containing aliphatic and aromatic amines

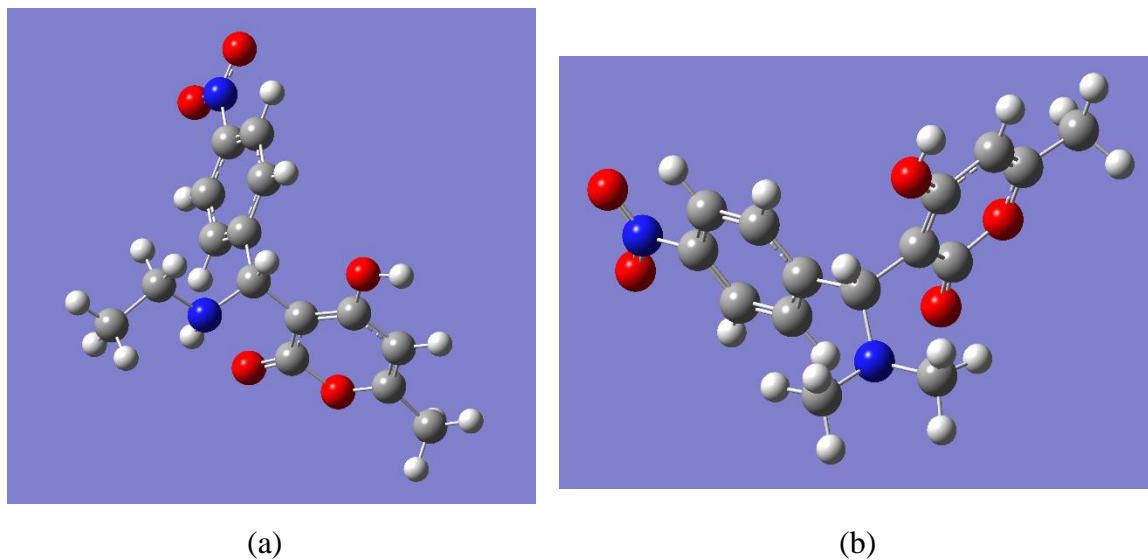
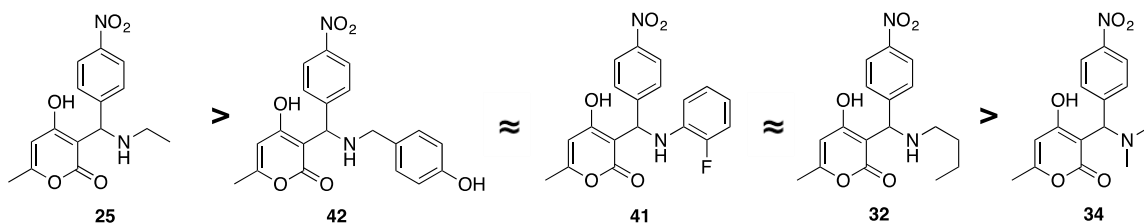


Figure 10: Optimized using HF/6-311+G(d,p). (a) Compound 25; (b) Compound 34.

Table 9: Corrosion inhibition activity of Mannich bases containing aliphatic and aromatic amine

| Entry | Compound | R _{ct} (Ohms) | %IE ± 2.5% |
|-------|----------|------------------------|------------|
| 1 | blank | *102.25 | 0 |
| 2 | 25 | 113.67 | 10.1 |
| 3 | 42 | 77.96 | -35.4 |
| 4 | 41 | 74.35 | -29.4 |
| 5 | 32 | 73.00 | -31.9 |
| 6 | 34 | 51.54 | -70.4 |



Scheme 9: Corrosion inhibition activity trend of Mannich bases containing aliphatic and aromatic amine

2.3 Conclusion

In this study, the corrosion inhibition activity of both small and complex organic molecules in mild steel was evaluated. The bio-based TAL and its derivatives showed appreciable anti-corrosion activity towards mild steel in Na₂SO₄ media. In terms of %IE, coumalic acid **54** was found to be the best 2-pyrone corrosion inhibitor. Substituted pyridines have also demonstrated anti-corrosion activity obtaining 30.0% and 29.5% inhibition efficiency by compounds **57** and **58**, respectively, the highest %IE attained in this work. This investigation was also extended from small molecules to highly functionalized Mannich bases. With the reaction conditions used in this study, TAL-derived Mannich bases promote corrosion rather than inhibit. It was proposed that the Mannich bases and Fe complex might be soluble. This results in the dissolution of the complex from the metal surface into the electrolyte solution, which exposes the active site to corrosion agents.

This chapter has explored the applications of the TAL derivatives in the area of corrosion science. Also, a set of N-heterocyclic compounds **58**, **60**, and **63** was recognized to inhibit corrosion in mild steel. To advance this study further, several suggestions were made. Firstly, in order to verify the governing interactions of small TAL-based inhibitors with the bulk metal, the effect of temperature in the %IE should be tested. If the %IE decreases with increasing temperature, then the inhibitor is physisorbed at the surface. If the %IE increases with temperature, then the inhibitor is chemisorbed at the surface. Secondly, to support the idea that TAL-derived Mannich bases form a soluble complex with Fe, UV-Vis spectroscopy could be done. Third, to validate the rationale for the observed trend, optimization of molecular geometry, especially the Mannich bases, should

be conducted. Lastly, organic compounds with similar structure that of *opuntiol* and the set of N-heterocycles should be screened for its anti-corrosion activity in metals.

2.4 Experimental

Materials

All starting materials including compounds **56**, **60**, **62**, **64**, **65**, **66**, TAL, and DAA were purchased from Sigma-Aldrich, Enamine, and TCI America. Solvents were purchased from Fisher Scientific and used without further purification. Mild steel samples containing 99.5% Fe, 0.2% Mn, 0.1% Cu, 0.04% C, 0.04% Ni, 0.03% Cr, 0.024% Si, 0.023% Al, 0.01% Mo, 0.008% P, 0.0073% N, 0.003% S, 0.003% Nb, 0.001% V, 0.001% Ti, and 0.0001% B, with a dimension of 0.5 cm X 3.0 cm X 0.1 cm were used. For electrochemical studies, mild steel strips with 0.5 cm² exposed surface area were employed. The mild steel samples were cleaned and abraded prior to testing.

Synthesis of Inhibitors

2-oxo-2H-pyran-5-carboxylic acid (54). The synthesis of **54** was adapted from the methods reported elsewhere.^[32] Briefly, In a solution of malic acid (9.3 mmol) and DCE (19 mL) added H₂SO₄(conc.) (46.6 mmol). The mixture was heated to 100⁰C for 16 hours, then, cooled down to room temperature. The resulting solution was poured onto ice and stirred. The crude product was extracted with EtOAc (3x). The organic fraction was washed with ice cold H₂O (3x), dried (MgSO₄), filtered, and concentrated in *vacuo*.

4-Methoxy-6-methyl-2H-pyran-2-one (56). The synthesis of **56** was adapted from the methods reported elsewhere.^[33] Briefly, to a solution of TAL (17.8 mmol) in acetone_(anhyd.) (55mL) was added K₂CO₃ (35.3 mmol). The resulting mixture was added Me₂SO₄ (21.1 mmol). The solution was refluxed and stirred for 3 hours. The crude product was poured onto NH₄Cl_(sat.) and extracted with EtOAc (2x). The organic fraction was dried (MgSO₄), filtered, and concentrated in *vacuo*.

6-(hydroxymethyl)pyridin-2-ol (58). The synthesis of **58** was modified from the methods reported elsewhere.^[34] Briefly, to a solution of **57** (3.75 mmol) and dry THF (20 mL) added BH₃-THF (19.0 mmol) at room temperature. The resulting mixture produced heat and was cooled down to room temperature. MeOH_(dry) was added and solution was heated to 65⁰C for 3.5 hours and concentrated in *vacuo*. Additional amount of MeOH (10 mL) was added and concentrated in *vacuo*.

5-(hydroxymethyl)pyridin-2-ol (60). The synthesis of **60** was employed with the same condition as the synthesis of **58**. Instead of **57**, compound **59** was used as starting material.

Mannich bases. The synthesis of Mannich bases was adapted from the method developed in the previous chapter. Briefly, to a dried flask TAL (1.0 mmol) was added. Stoichiometric amount of aldehyde (1.0 mmol) was added, followed by the addition of DMM (5-6 mL). To this suspension, amine (1.0 mmol) was added and stirred. The resulting solution was added a catalytic amount of AcOH (1 mol%). Mixture was stirred at room temperature

overnight. The precipitate was filtered, washed with petroleum ether (1 mL x 10), and dried in air.

Characterization of Inhibitors

Structure determination of inhibitors was employed with ^1H and ^{13}C NMR spectroscopy in CDCl_3 or DMSO-d on a Varian 400 MR or Bruker AVIII 600 MHz spectrometer. ^1H and ^{13}C chemical shifts (δ) are given in ppm relative to the residual protonated solvent peaks (CDCl_3 : $\delta_{\text{H}} = 7.26$ ppm, $\delta_{\text{C}} = 77.2$ ppm; DMSO-d : $\delta_{\text{H}} = 2.50$ ppm, $\delta_{\text{C}} = 39.5$ ppm) as an internal reference. Low-resolution mass spectra (LRMS) were recorded on an Agilent 6540 QTOF (quadrupole time of flight) mass spectrometer using ESI (electrospray ionization) or APCI (atmospheric-pressure chemical ionization) or EI (electron ionization) on an Agilent 6890 GC/MS.

Preparation of Buffer -Inhibitor solution

In an Erlenmeyer flask, 0.1 M $\text{Na}_2\text{SO}_4(\text{anhyd.})$ in deionized H_2O (18.2M Ω) was added with an amount of the inhibitor (1.0 mmol). The resulting mixture was stirred and sonicated to obtain a homogenous mixture. The pH was adjusted between 2.70-2.80 with $\text{H}_2\text{SO}_4(\text{conc.})$ using a handheld pH meter.

Electrochemical Studies

The EIS curves were generated using electrochemical analyzer with a built-in software. A three-electrode cell setup consisting a reference electrode (Ag/AgCl), counter electrode (Pt with glass tube), and working electrode (mild steel with exposed surface area

in the corrosive buffer system of 0.5 cm² was used. The working electrode was abraded with 300 and 1200 grade sand papers and washed with DI water prior to each testing. All tests were conducted at temperature between 21⁰C – 22⁰C without stirring. For each EIS experiment, the working electrode was immersed in the acidic medium for 30 min. and its OCV was recorded at that time interval. The steady state OCV of the working electrode was consistently achieved after 30 min. of immersion. EIS curves were recorded at OCV values with 10000-0.1 Hz frequency range. The impedance curves in the Nyquist plots were generated using EC Lab V10.02 software. The impedance curves were assumed to fit the Simplified Randles Cell model circuit.

2.5 References

- [1] Jeeva, M.; et al., *J. Phys. Chem. C*, **2015**, *119*, 22025–22043.
- [2] Dasami, P.M.; et al., *Orient. J. Chem.*, **2015**, *31(1)*, 185-191.
- [3a] Gajda-Scharantz, K.; et al., *Phys. Chem. Chem. Phys.*, **2013**, *15*, 1443-1451.
- [3b] Wei, L.; et al., *J. Cryst. Growth*, **2012**, *342*, 21-27.
- [4] Beverskog, B.; Puigdomenech, I., *Corrosion Science*, **1996**, *38(12)*, 2121-2135.
- [5] Raja, P.B.; et al., *Surf. Rev. and Lett*, **2015**, *22(3)*, 1-8.
- [6] Zhao, X.; et al., *Sensors*, **2011**, *11*, 10798-10819.
- [7] Neville, A., *Mater. and Struct.*, **1995**, *28*, 63-70.
- [8] De Schutter, G.; Luo, L., *Constr. Build. Mater.* **2004**, *18*, 483–489.
- [9] Sato, N.; *Green Corrosion Chemistry and Engineering: Opportunities and Challenges*, Wiley-VCH Verlag GmbH & Co. KGaA, 2012.
- [10] Raja, P.B.; Sethuraman, M.G., *Mater. Lett.*, **2008**, *62*, 113-116.
- [11] Yadav, D.K.; Quraishi, M.A., *Ind. Eng. Chem. Res.*, **2012**, *51*, 8194-8210.

- [12] Gopi, D.; et al., *Ind. Eng. Chem. Res.*, **2014**, *53*, 4286-4294.
- [13] Kovacevic, N.; Kokalj, A., *J. Phys. Chem C.*, **2011**, *115*, 24189-24197.
- [14] Donya, A.P.; et al., *Prot. of Met.*, **2002**, *38(3)*, 216-219.
- [15] Harvey, T.G.; et al., *Corrosion Science*, **2011**, *53*, 2184-2190.
- [16] William, G.; et al., *Electrochim. Acta*, **2010**, *55*, 5947-5958.
- [17] Bockris, J.; Swinkels, A.; *J. Electrochem. Soc.* **1964**, *111(6)*, 736-743.
- [18] Ostovari, A.; et al., *Corros. Sci.*, **2009**, *51*, 1935-1949.
- [19] Jeeva, M.; et al., *J. Phys. Chem. C*, **2015**, *119*, 22025-22043.
- [20] Khan, G.; et al., *Int. J. Electrochem. Sci.*, **2015**, *10*, 6120 - 6134.
- [21] Ahmad, Z. *Principles of Corrosion Engineering and Corrosion Control*; Elsevier Science & Technology Books: New York, 2006.
- [22] Gupta, M.; et al., *Int. J. of Corr.*, **2013**, *582982*, 1-5.
- [23] Singh, D.K.; et al., *J. of Molec. Liq.*, **2016**, *216*, 738-746.
- [24] Loto, R.T.; et al., *J. Mater. Environ. Sci.*, **2012**, *3(5)*, 885-894.
- [25] Namoussa, E.Y.; et al., *Chem. Sci. Trans.*, **2015**, *4(4)*, 961-966.
- [26] Ekanem, U.F.; et al., *J. Mater. Sci.*, **2010**, *25(45)*, 5558-5566.
- [27] Ma, C.; et al., *J Chromatogr A*, **2007**, *39*, 1165.
- [28] Loganayagi, C.; et al., *ACS Sust. Chem. Eng.*, **2014**, *2(4)*, 606-613.
- [29] Wadsworth, A.D.; et al., *Synthesis*, **2010**, *15*, 2604-2608.
- [30] Bacardit, R.; et al., *J. of Hetero. Chem.*, **1982**, *19(1)*, 157-60.
- [31] Hnini, K., et al., *Leonardo Electronic J. Pract. and Techn.*, **2008**, *12*, 1-14.
- [32] Pollock, G., Graduate Thesis and Dissertations, Iowa State University, 2013, paper 13479.

[33] Wadsworth, A.D.; et al., *Synthesis*, **2010**, *15*, 2604-2608.

[34] Bridger, G.; et al., PCT Int. Appl., 2011012622, 03 Feb 2011.

CHAPTER III

GENERAL CONCLUSION

The versatility of the bio-based triacetic acid lactone as a platform chemical and the application of its derivatives have been explored. Chapter 1 of this thesis emphasized the development of an efficient method for the Mannich reaction of triacetic acid lactone. Despite the downside of obtaining Mannich bases with lower yields than previously reported, the method developed has several advantages. First, it promotes the use of cheap and benign acetic acid as the catalyst. Second, it eliminates the use of high percent loading of the catalyst. Finally, it demonstrates the ability of triacetic acid lactone to produce sustainable molecularly diverse molecules.

Chapter 2 of this work evaluated the corrosion inhibition activity of the bio-based triacetic acid lactone derivatives, selected pyridines, and TAL-derived Mannich bases. Triacetic acid lactone and its derivatives have demonstrated anti-corrosion activity in mild steel under acidic condition. The Mannich base derivatives, on the other hand, have resulted in the promotion of the corrosion activity rather than inhibition. This study has also led to the discovery of new set of N-heterocyclic compounds that inhibit corrosion in metal. Further tests have to be conducted to investigate the effects of molecular structure, temperature, and inhibitor concentration to the corrosion inhibition efficiency of these compounds in the current study.